Land cover classification and -monitoring of the Austrian Biosphere Reserves based on satellite data (BRmon)

Final Report

Michael Lechner & Markus Immitzer

150 YEARS FEATURING FUTURE 1872 - 2022

UNIVERSITY OF NATURAL RESOURCES AND LIFE SCIENCES, VIENNA

Project manager

Dr. Markus Immitzer

University of Natural Resources and Life Sciences, Vienna (BOKU)

Department of Landscape, Spatial and Infrastructure Sciences

Institute of Geomatics

Project duration

01.10.2019 – 31.03.2022

Content

1. Introduction and Objectives of the project

Based on the experiences and results of the FFG-funded project 'EO4Forest' (https://www.rali.boku.ac.at/ivfl/themenfelder/fernerkundung-forstwirtschaft/ffg-asap-projekt-eo4forest/), the main goal of **BRmon** is the extension of the mapping in scale, time and level of detail.

Based on Copernicus data, mainly Sentinel-2, the land cover of all Austrian biosphere reserves (BRs): BR *Wienerwald,* BR *Großes Walsertal* and BRs *Salzburger Lungau* and *Kärntner Nockberge* are classified. These results can be used as baseline for operational monitoring programs and can serve as an input for related research.

In the BR *Wienerwald* the level of detail in terms of analyzed classes is extended. Additional reference data for tree species and grassland areas are collected. As a result, the number of identified tree species will increase and information about mowing and forest management activities (and calamities) are provided. Next to Sentinel-2 also Sentinel-1 data provided by colleagues from the TU Vienna was used.

For the temporal extension back to 1980s, data from the Landsat data archive are used. Landsat data with a spatial resolution of 30 m (compared to 10/20 m of Sentinel-2) are available from 1982 (Landsat 4 and 5). Using those data, the historical land cover development of the BRs is analyzed.

Based on the outcomes of the individual activities, the potential of the Copernicus data (i.e. Sentinel-2) for land cover mapping and monitoring of Austrian BRs are evaluated and a monitoring concept is formulated.

Detailed objectives of the research project are as follows:

- **Objective 1:** Land cover maps for all Austrian BRs:
  BR *Wienerwald,*
  BR *Großes Walsertal* and
  BRs *Salzburger Lungau and Kärntner Nockberge.*
- **Objective 2:** Detailed land cover analysis (tree species, mowing activities) for the BR *Wienerwald.*
- **Objective 3:** Test of transferability of the developed models for detailed land cover mapping to other regions (BR *Großes Walsertal* and BRs *Salzburger Lungau and Kärntner Nockberge*)
- **Objective 4:** Historical developments of the land cover of all Austrian BRs.
- **Objective 5:** Monitoring possibilities and monitoring concept for all Austrian BRs.

Figure 1 shows the locations of the four Austrian BRs together in relation to the different Sentinel-2 orbits. The BR *Wienerwald* and the BRs *Salzburger Lungau* and *Kärntner Nockberge* are in the swath-overlap of two different Sentinel-2 orbits. Every five days one of the two Sentinel-2 satellites collect data in the same orbit. Therefore, the temporal resolution in the overlap areas is two scenes in five days. In contrast, BR *Großes Walsertal* is only covered by the swath of a single Sentinel-2 orbit; consequently, a single scene will be acquired every 5 days.
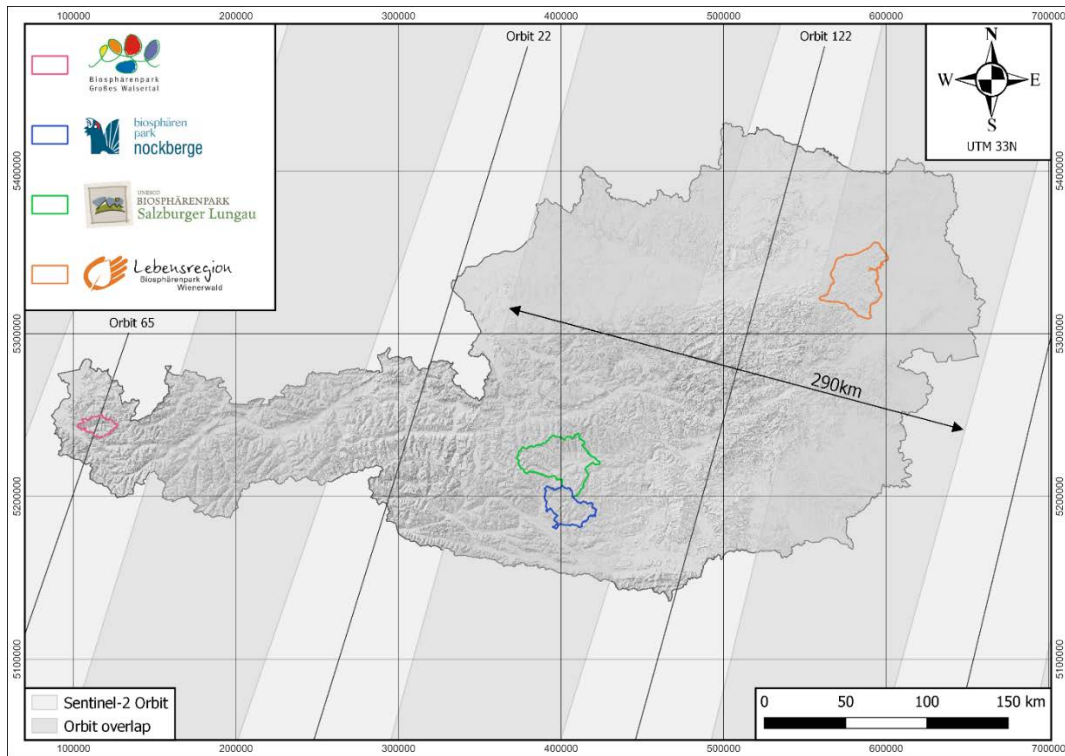
Figure 1: Location of Austrian Biosphere Reserves and Sentinel-2 orbit cover and overlap (background: hill shaded digital terrain model).

Not only does the data availability differ for Austrian BRs, also the topographic situation is very different. BR *Wienerwald* is located on the foothill of the Northern Alps located west of Vienna. The landscape is characterized by wooded hills alternating with meadows, pastures, vineyards, and dry grasslands. In contrast, the landscapes of the other BRs are dominated by alpine forests and grasslands; large differences in altitude exist. Mountainous areas pose various challenges to satellite-based remote sensing, especially the negative influence of cast shadows (during the winter season), the duration of snow cover, and the generally higher probability of clouds in alpine environments. All the aforementioned circumstances influence the amount of Sentinel-2 data useful for analysis of the different BRs.

Figure 2 shows an overview of the project work packages and activities separated for the three biosphere reserves. All planned work could be implemented in the course of the project. Only the transferability tests were not possible due to insufficient reference data and the significantly worse data situation regarding reference data.

Land cover classification and -monitoring of the Austrian biosphere reserves based on satellite data
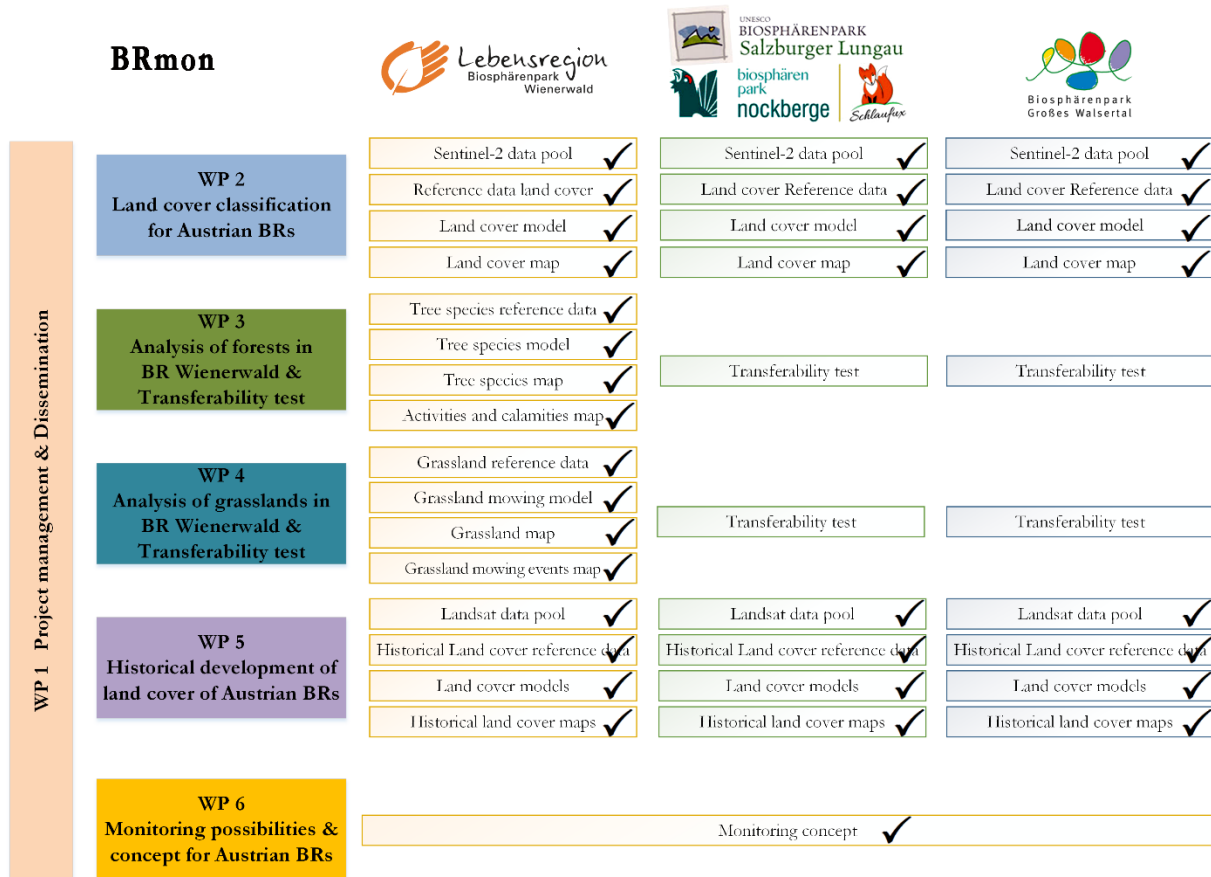
Figure 2: Overview of the Project: Work packages (WPs) and Activities for the three different biosphere reserves (BRs).

For the dissemination a project webpage with information about the project were launched at the BOKU (https://boku.ac.at/rali/geomatics/themenfelder/fernerkundung-wald/oeaw-projekt-brmon) and the Biosphärenpark Wienerwald (biosphere reserve Wienerwald) webpage. The project and also first results were presented at BPWW Forschungstag – a stakeholder workshop with several interest groups. After the presentation was plenty of time for a fruitful discussion with potential users for the produced data, both at university level as well as practitioners (such as *Biosphärenpark Botschafter*).

The presentation of some results in the journal of BR Wienerwald is planned for the second half of 2022.

The combination of Sentinel-1 and Sentinel-2 for tree species classification was published in Remote Sensing (https://doi.org/10.3390/rs14112687). It is planned to present the results also at the scientific conference ForestSAT in Berlin (Sep. 2022).

Michael Lechner wrote his master's thesis in the course of the project and performed additional analyses. The thesis was completed in May 2022.

2. Land cover maps for all Austrian BRs (WP 2)

Based on images from the Copernicus' Sentinel-2 satellites, land cover classifications were created for the Austrian biosphere reserves. For this purpose, a 1 km point grid was superimposed on the BR *Wienerwald* and the BRs *Salzburger Lungau* and *Kärntner Nockberge*. Due to the smaller spatial extent of the BR *Großes Walsertal*, the grid was reduced to 0.5 km here.

Due to the lack of reference information these points were visually interpreted using orthophotos. This worked very well for the BR *Wienerwald* but in the two mountains BR was due to the topography the interpretation partly difficult.

Table 1 shows the land cover classes principally considered for land cover analysis for the three study areas. Sample images for the land cover classes from the BR *Großes Walsertal* at three different time steps are presented in Figure 3 .

For the BR *Wienerwald* and the BRs *Salzburger Lungau* and *Kärntner Nockberge*, data from the forestry enterprises were additionally used to sharpen the quality of the samples. Classes with only a few samples were then further condensed. Thus, 781 training pixels were obtained for the BR *Wienerwald*, 714 for the BR *Großes Walsertal* and a total of 1645 training pixels for the BRs *Salzburger Lungau* and *Kärntner Nockberge* (Figure 4 – Figure 6).

Table 1: Class descriptions for the land cover classification analysis and sample number for the three biosphere reserves (BRWW: BR *Wienerwald*, BRGW: BR *Großes Walsertal*, BRSLNK: BRs *Salzburger Lungau* and *Kärntner Nockberge*).

Class	Definition	BRWW	BRGW	BRSLNK
Broadleaved forest	broadleaf-dominated forest	384	53	61
Needleleaved forest	conifer-dominated forest	97	117	729
Mixed forest	Mixed coniferous and broadleaf forest	-	83	99
Dwarf pine	Dwarf mountain pine (*Pinus mugo*) dominated forest	-	-	47
Farmland	Crop cultivation, vine yards	76	-	-
Grassland	Grassland, meadows, lawns, pastures, parks, etc.	103	282	466
Rock	Bare rock and stone	-	104	123
Built-up areas	Sealed surfaces - buildings, roads and other infrastructure	107	62	68
Water bodies	Lakes, rivers, ponds, etc.	14	-	52
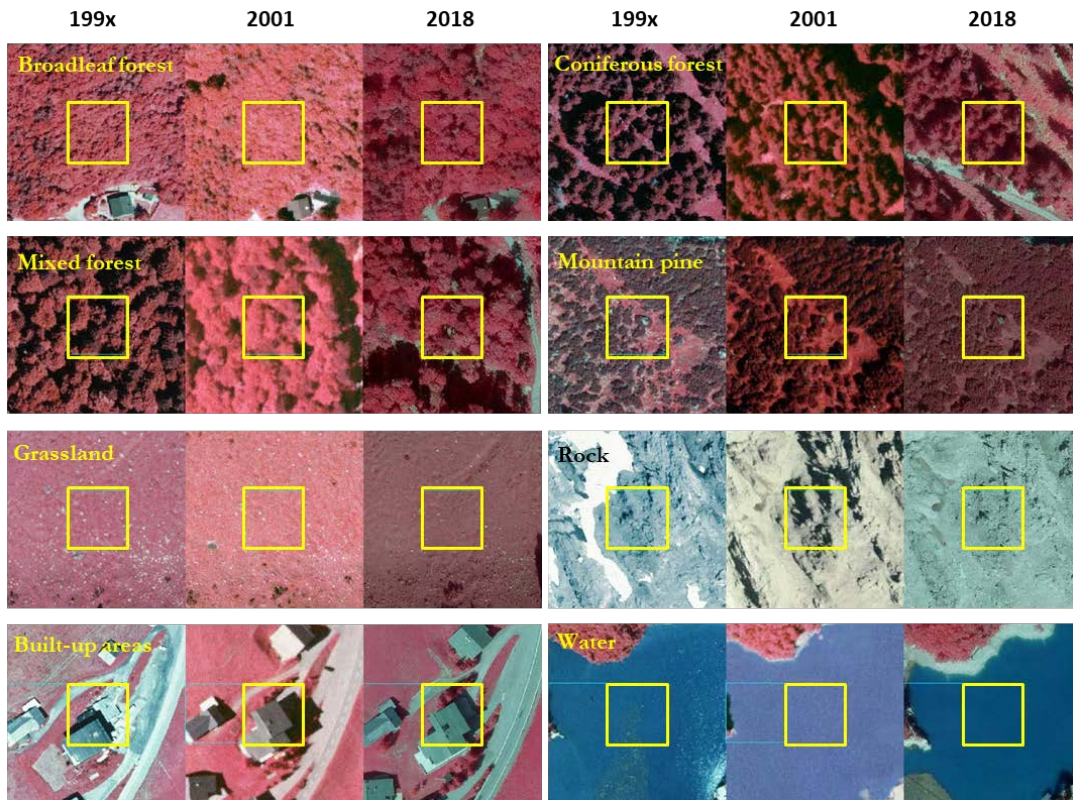
Figure 3. Examples of classes considered for the land cover classification for three different time steps: 199x, 2001 and 2018 (CIR composite orthoimages) for the BR *Großes Walsertal*.
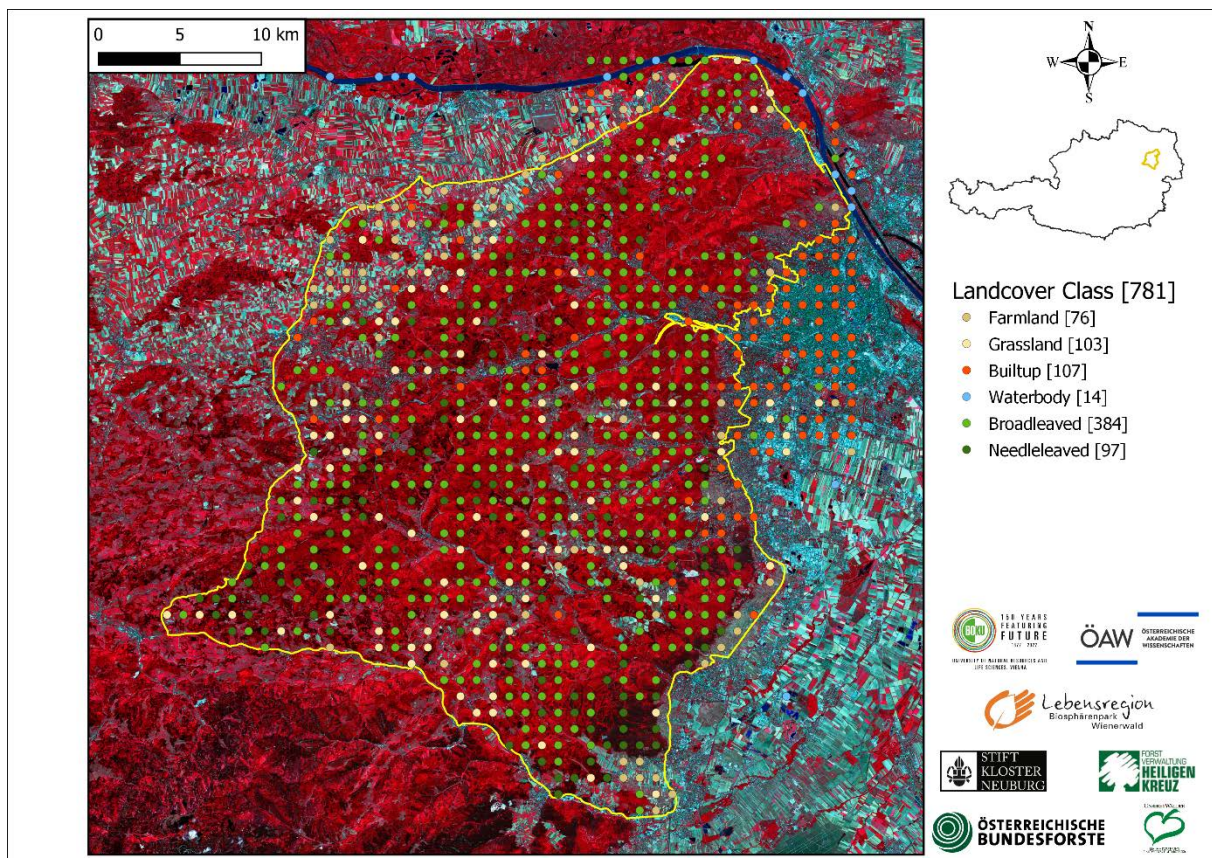
Figure 4: Sample points (n= 781) representing the land cover classes, created for the BR *Wienerwald* by use of orthophotos and data from forestry enterprises.

Figure 5: Sample points (n=714) representing the land cover classes, created for the BR *Großes Walsertal* by use of orthophotos
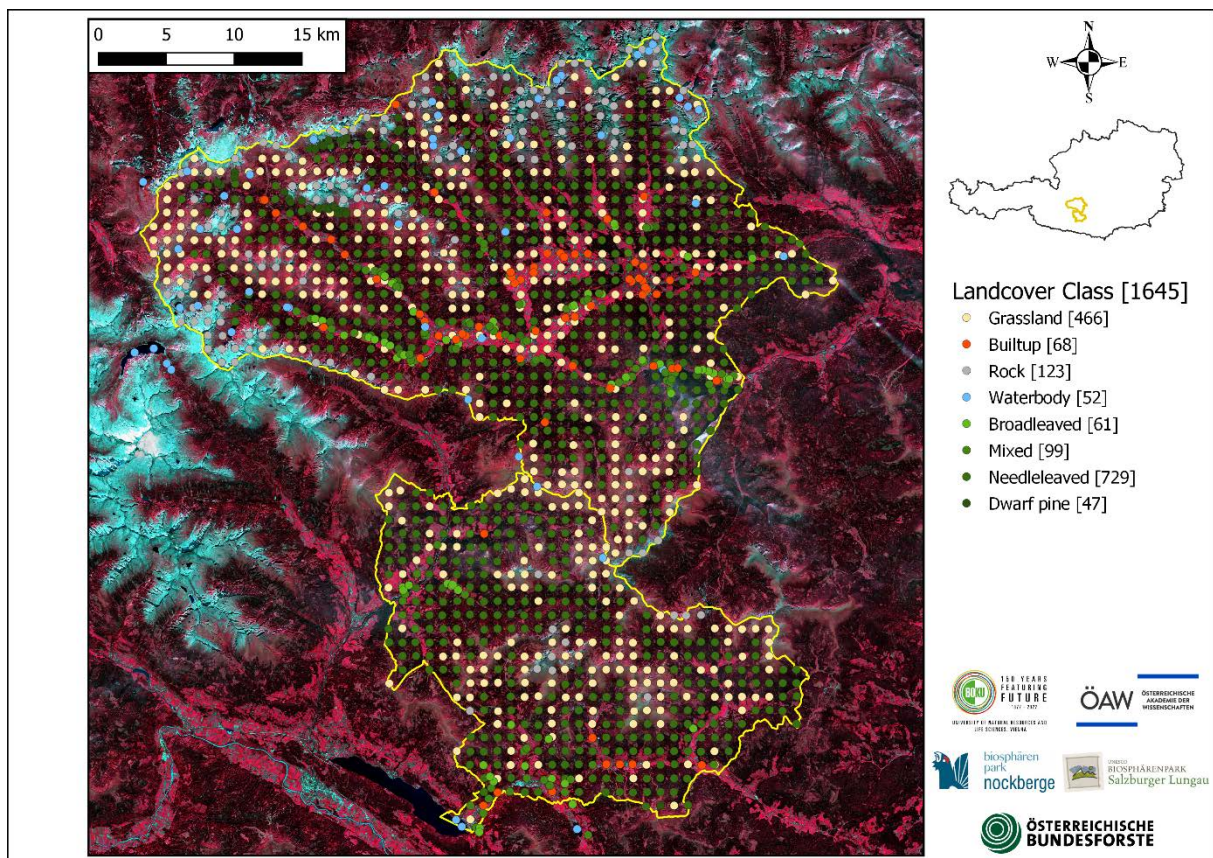
Figure 6: Sample points (n=1645) representing the land cover classes, created for the BRs *Salzburger Lungau* and *Kärntner Nockberge* by use of orthophotos and data from forestry enterprises

All available Sentinel-2 scenes were visually checked for their suitability for classification. Exclusion criteria were clouds and snow cover. An overview of the used scenes can be found in Table 2.

Due to the orbital location, a total of 46 scenes are available at BR *Wienerwald*. Although BR *Salzburger Lungau* and *Kärntner Nockberge* is also favoured here, only seven scenes are suitable here due to its spatial size and inner-alpine location. For the BR *Großes Walsertal*, seven suitable scenes could also be identified. Furthermore, the BRs *Salzburger Lungau* and *Kärntner Nockberge* is in the cross-region of four Sentinel-2-tiles, which made it necessary to mosaic these.

Table 2: Overview of the used Sentinel-2-scenes used for the land cover-classification of each BR. (** have been created as a quad-mosaic of tiles 33TUM/33TUN/33TVM/33TVN)

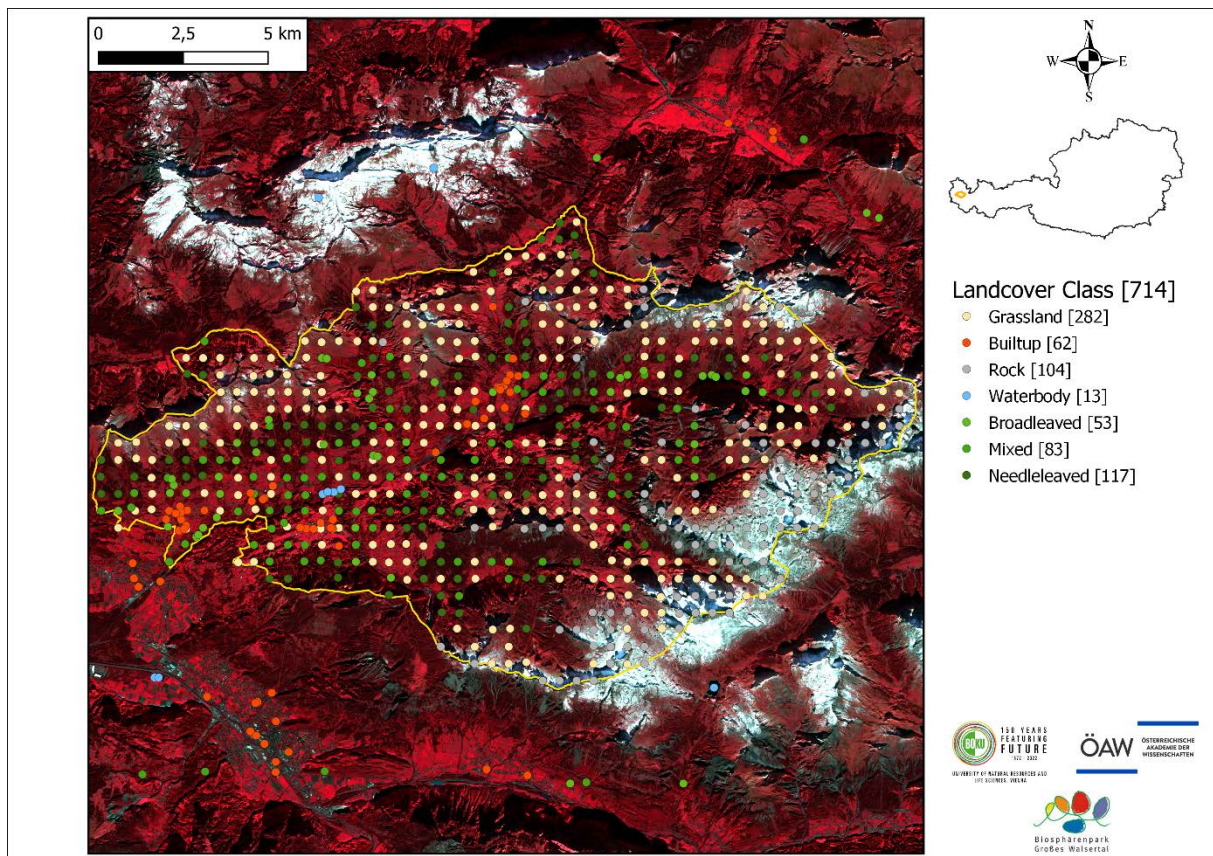| BR *Wienerwald*		BR *Großes Walsertal*	BRs *Salzburger Lungau* and *Kärntner Nockberge*
33UWP_122_2017-04-01	33UWP_122_2020-09-12	32TNT_65_2017-06-26	33T**_122_2018-09-28
33UWP_122_2017-06-20	33UWP_79_2017-05-18	32TNT_65_2017-08-25	33T**_122_2018-10-13
33UWP_122_2017-08-29	33UWP_79_2017-05-28	32TNT_65_2017-10-14	33T**_122_2019-09-13
33UWP_122_2017-09-08	33UWP_79_2017-08-01	32TNT_65_2018-10-14	33T**_22_2017-10-16
33UWP_122_2017-09-28	33UWP_79_2017-08-31	32TNT_65_2019-09-04	33T**_22_2019-09-21
33UWP_122_2018-04-21	33UWP_79_2017-09-30	32TNT_65_2019-09-29	33T**_22_2019-10-26
33UWP_122_2018-05-06	33UWP_79_2017-10-15	32TNT_65_2020-07-10	33T**_22_2020-09-05
33UWP_122_2018-08-09	33UWP_79_2018-04-08		
33UWP_122_2018-08-29	33UWP_79_2018-07-02		
33UWP_122_2018-09-13	33UWP_79_2018-08-21		
33UWP_122_2018-09-18	33UWP_79_2018-09-30		
33UWP_122_2018-09-28	33UWP_79_2018-10-05		
33UWP_122_2018-10-13	33UWP_79_2018-10-10		
33UWP_122_2019-04-01	33UWP_79_2018-10-30		
33UWP_122_2019-04-16	33UWP_79_2019-08-31		
33UWP_122_2019-04-21	33UWP_79_2019-09-15		
33UWP_122_2019-06-30	33UWP_79_2020-04-02		
33UWP_122_2019-07-20	33UWP_79_2020-04-07		
33UWP_122_2019-07-25	33UWP_79_2020-04-12		
33UWP_122_2019-08-09	33UWP_79_2020-04-22		
33UWP_122_2020-04-05	33UWP_79_2020-07-31		
33UWP_122_2020-08-08	33UWP_79_2020-09-09		
33UWP_122_2020-08-28	33UWP_79_2020-10-04		

Based on these trainings data classification models were created. Therefore, the machine learning algorithm random forest (Breiman, 2001) were used, which is based on an ensemble of independent decision trees. The implemented bootstrapping provides a reliable measure of the quality of the model, the so-called out of bag (OOB) result. One additional advantage of the algorithm is the implanted evaluation of the variable importance such as the Mean-decrease-in-Accuracy value. To improve the model-quality, a recursive feature selection using the variable importance values was applied for all models (Immitzer et al., 2019, 2018). The results of the OOB-classifications are listed in Table 3 – Table 5.

The highest overall accuracy (OA) with 95.6% was achieved for the BR *Wienerwald*, which can be explained by the doubled temporal resolution and the thus increased available image data. The six predefined classes could be separated very well by the classification model, the best results were achieved by the classes broadleaved (producer's accuracy (PA) = 98.4%, user's accuracy (UA) = 97.7%) and waterbody (PA = 100%, UA = 100%). The classes farmland (PA = 88.2%, UA = 93.1%) and grassland (PA = 90.3%, UA = 88.6%), which also showed the lowest user and producer accuracies, proved to be the most difficult to separate.

Table 3: Confusion matrix based on the OOB-result of the BR *Wienerwald* land cover classification (UA: user's accuracy, PA: producer's accuracy, OA: overall accuracy)

BRWW - S2
Land cover

	farmland	grassland	built-up	waterbody	broadleaved	needleleaved	UA
farmland	**67**	2	3	0	0	0	93.1%
grassland	8	**93**	0	0	4	0	88.6%
built-up	1	4	**103**	0	1	0	94.5%
waterbody	0	0	0	**14**	0	0	100%
broadleaved	0	4	0	0	**378**	5	97.7%
needleleaved	0	0	1	0	1	**92**	97.9%
PA	88.2%	90.3%	96.3%	100%	98.4%	94.8%	
				$\varkappa =$	0.937	**OA =**	**95.6%**

The model was then applied to the entire area of the BR *Wienerwald* and a map of the land cover classes was created, which is shown in Figure 7. The heavily populated areas of the outskirts of Vienna and the areas around the western highway to the east into the *Tullner Becken,* as well as individual populated areas within the BR *Wienerwald*, are clear eyecatchers. The dominance of deciduous forest stands in the entire area and the coniferous regions in the southeast and in the western part of the BR are also clearly noticeable.
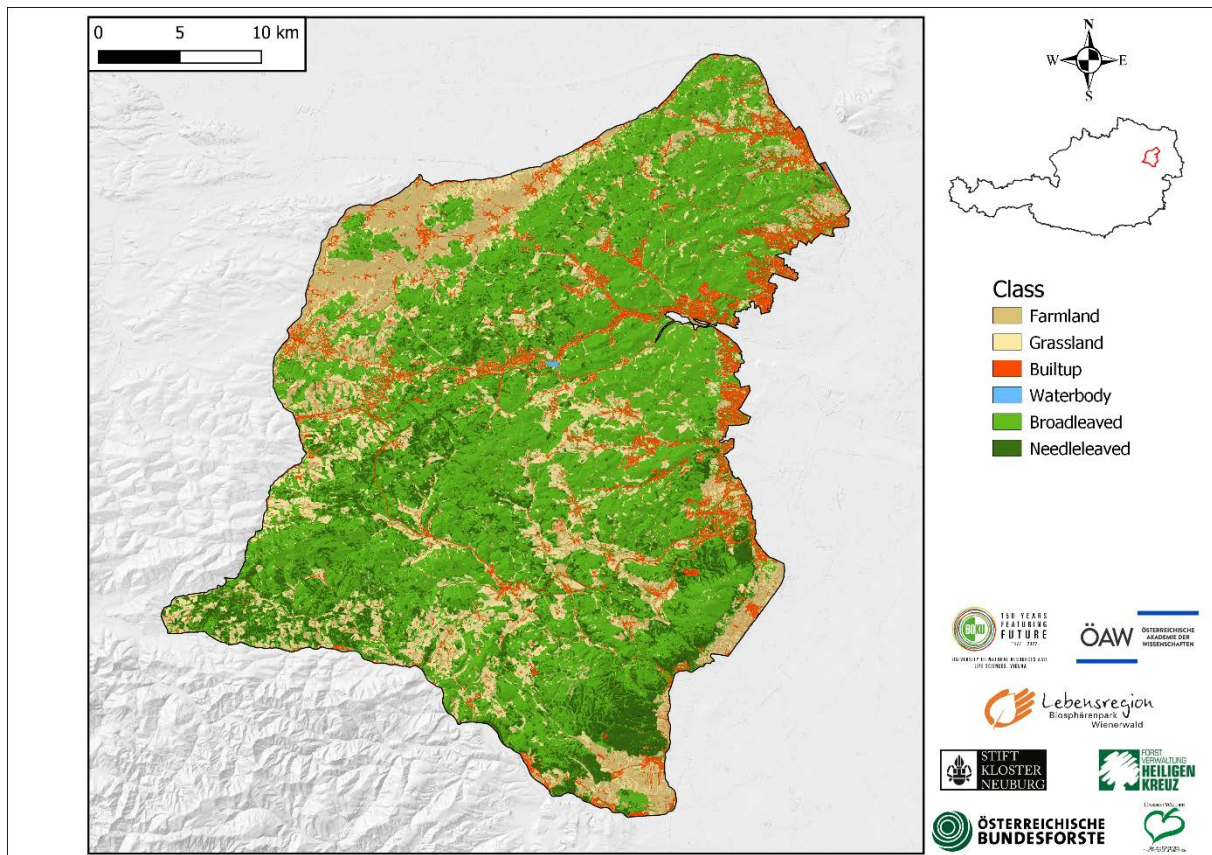
Figure 7: Land cover map of the BR *Wienerwald* based on Sentinel-2-imagary from 2017-2020.

With an overall accuracy of OA = 87.8%, the result of the BR *Großes Walsertal* classification model was somewhat lower. This was mainly caused by the classes broadleaved (PA = 86.3%, UA = 71.7%), grassland (PA = 71.7%, UA = 95.5%) and waterbody (PA = 57.8%, UA = 100%). For broadleaved and waterbody, this can be explained by the few training pixels represented. Nevertheless, we can speak of very good classification results for this model as well.

Table 4: Confusion matrix based on the OOB-result of the BR *Großes Walsertal* land cover classification (UA: user's accuracy, PA: producer's accuracy, OA: overall accuracy)

BRGWT - S2								
	grassland	built-up	rock	waterbody	broadleav.	mixed	needleleav.	UA
grassland	**274**	2	2	0	1	3	5	95.5%
built-up	0	**54**	2	0	0	0	0	96.4%
rock	2	6	**99**	0	0	0	0	92.5%
waterbody	0	0	0	**13**	0	0	0	100%
broadleaved	0	0	0	0	**38**	14	1	71.7%
mixed	0	0	0	0	13	**48**	10	67.6%
needleleaved	6	0	1	0	1	18	**101**	79.5%
PA	71.7%	87.1%	97.2%	57.8%	86.3%	95.2%	100%	
						$\varkappa =$	0.841	**OA =** 87.8%

While almost half of the BR *Großes Walsertal* consists of grassed areas, it is easy to see that the forest areas are, due to the altitude, mainly coniferous forest dominated areas (Figure 8).

Areas of deciduous forest can be found especially at lower altitudes and on the slopes of the valleys. Due to the spectral similarity of the classes built-up and rock, a relatively large number of rock formations were identified as settlements in a false-negative way, which leads to an overestimation of the built-up areas as well as to an underestimation of the rock surface in the BR.
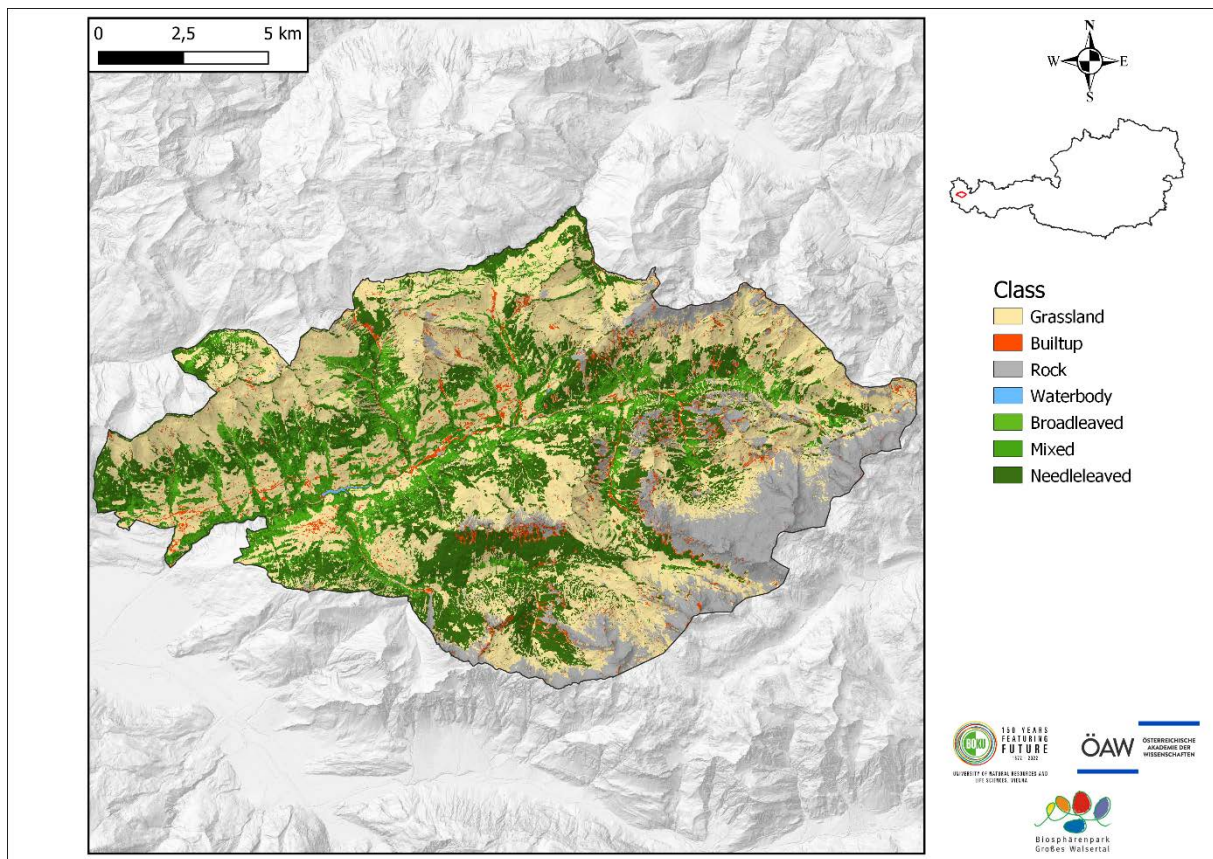
Figure 8: Land cover map of the BR *Großes Walsertal* based on Sentinel-2-imagery from 2017-2020.

The classification model of the BRs *Salzburger Lungau* and *Kärntner Nockberge* achieved an OA of 91.1%, whereby all classes of the OOB samples could be separated well throughout. Outliers are the classes broadleaved (PA = 73.8%, UA = 77.6%) and mixed, (PA = 56.6%, UA = 80.0%) which are potentially underrepresented due to the predominant forest communities in the BR.

Table 5: Confusion matrix based on the OOB-result of the BRs *Salzburger Lungau* and *Kärntner Nockberge* land cover classification (UA: user's accuracy, PA: producer's accuracy, OA: overall accuracy)

BRSLKN - S2

	grassland	built-up	rock	waterbody	broadleav.	mixed	needleleav.	dwarf pine	UA
grassland	**452**	2	4	0	1	1	18	2	94.2%
built-up	1	**57**	7	0	0	0	0	0	87.7%
rock	3	9	**110**	1	0	0	1	0	88.7%
waterbody	0	0	1	**50**	0	0	0	0	98.0%
broadleav.	1	0	0	0	**45**	12	0	0	77.6%
mixed	0	0	0	0	9	**56**	4	1	80.0%
needleleav.	9	0	1	1	6	30	**705**	20	91.3%
dwarf pine	0	0	0	0	0	0	1	**24**	96.0%
PA	97.0%	83.8%	89.4%	96.2%	73.8%	56.6%	96.7%	51.1%	
						$\varkappa =$	0.873	**OA =**	**91.1%**

In the land cover map of the BRs *Salzburger Lungau* and *Kärntner Nockberge,* shown in Figure 9, these clearly have coniferous forest character. Deciduous and mixed forests are found only sporadically, and at higher altitudes, European mountain pine can also be found. The centers of settlement are found on the one hand in the Salzburg area around *St. Michael* to *Tamsweg*, and on the other hand in the Carinthian *Gegental* east of the *Millstätter See*. The *Tauern* motorway, which formally cuts off part of the park in the western part of the Carinthian area, is also clearly recognizable.

In the area of the *Hohe Tauern*, similar to the BR *Großes Walsertal*, rock formations wrongly classified as built-up are detectable.
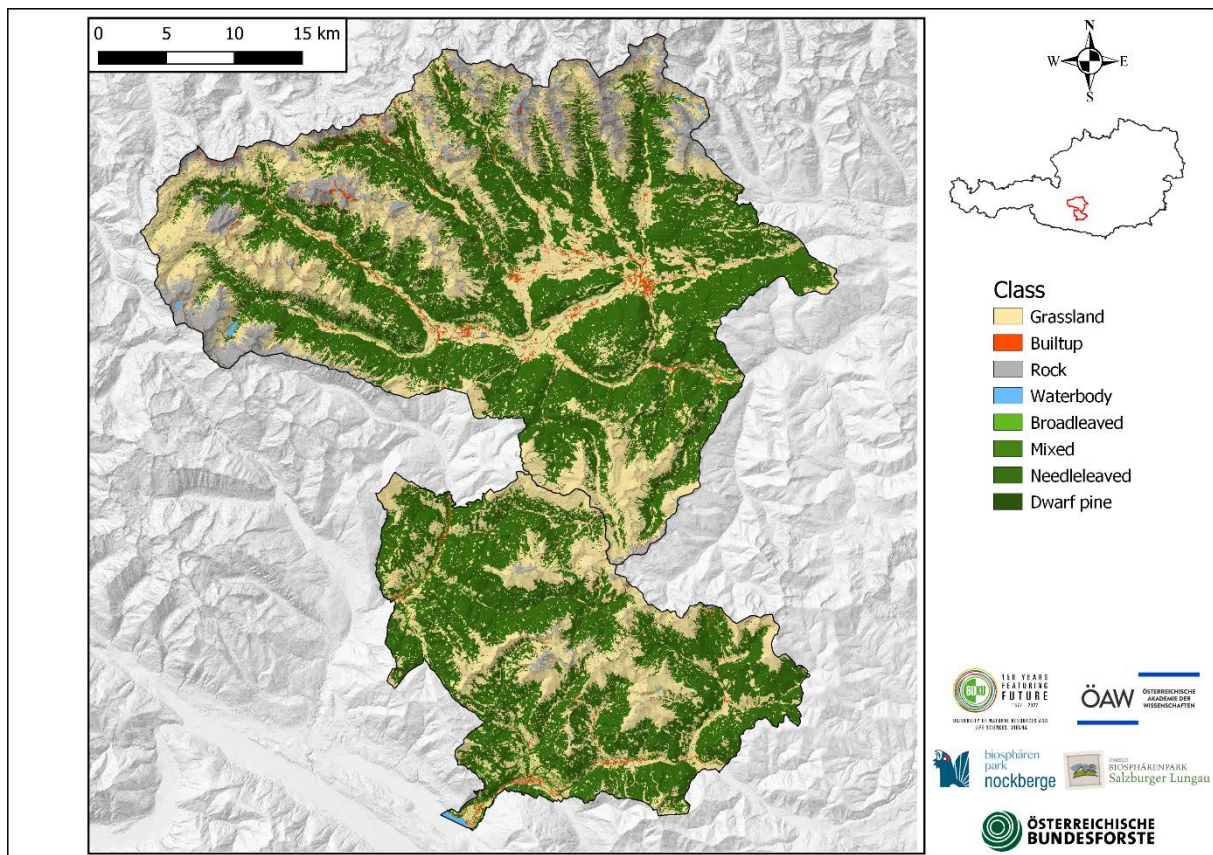
Figure 9: Land cover map of the BRs *Salzburger Lungau* and *Kärntner Nockberge* based on Sentinel-2-imagery from 2017-2020.

3. Detailed land cover analysis for the BR *Wienerwald* (WP 3)

For the tree species classification of BR *Wienerwald*, 1283 training pixels were collected with the help of data from the local forestry enterprises, which are shown in Figure 10. These represent seven deciduous and five coniferous tree species. For the classification itself, only the Sentinel-2-data of the 2018 vegetation period were used, as the results of the classification model are to be compared with a classification containing data from the Sentinel-1 satellite pair only from the same year. In contrast to the Sentinel-2 satellites, which measure reflected light in the visible to short-wavelength infrared domain, these satellites, also provided by the Copernicus programme of the EU, using radar sensors. This active imaging technology allows for the acquisition of data useful for remote sensing even in the presence of atmospheric conditions such as cloud cover. The Sentinel-1 data was provided by the Vienna University of Technology (TU Vienna).
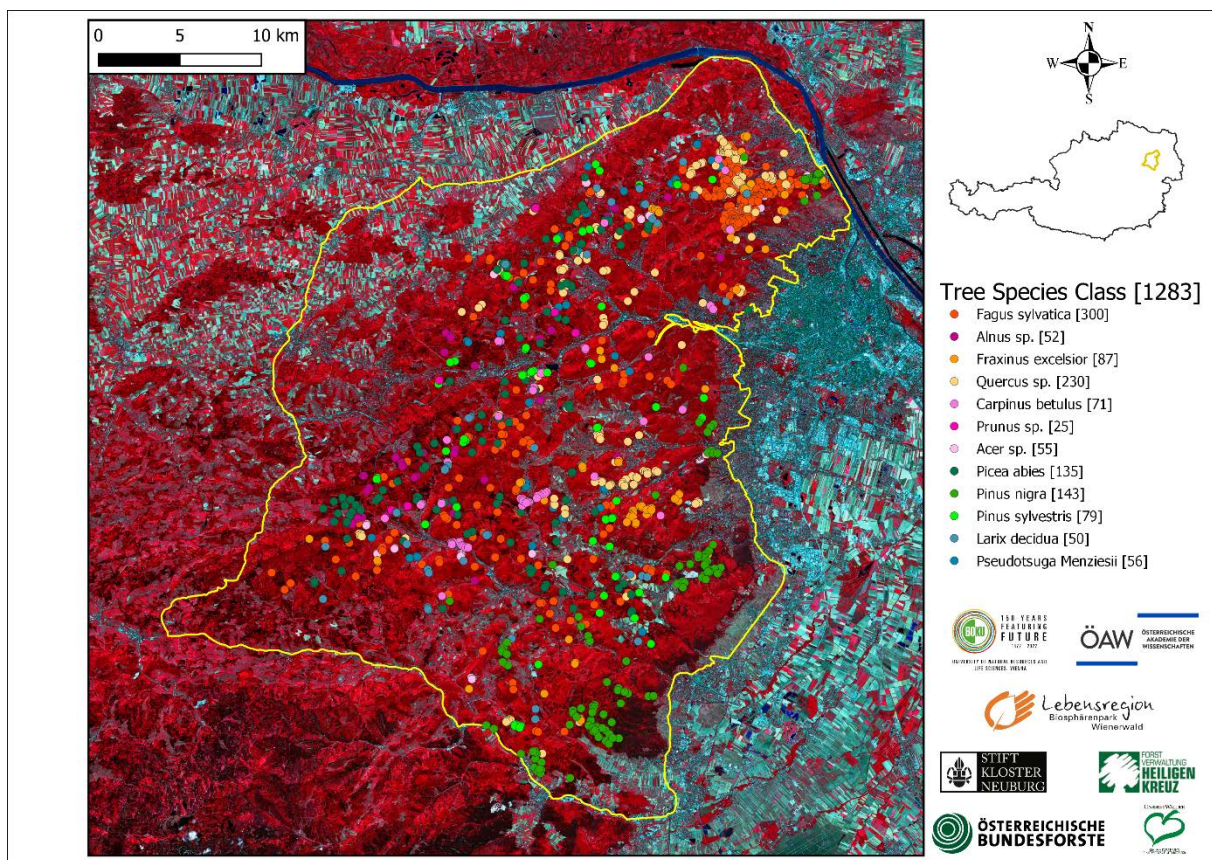
Figure 10: Sample points (n=1283) representing the tree species, created for the BR *Wienerwald* by use of orthophotos and data from forestry enterprises

By using Sentinel-2 data listed in Table 6, one tree species classification for the entire forest area of the BR *Wienerwald* was done. For the classification 14 Sentinel-2 scenes from the vegetation season of 2018 were used.

Table 6: Detailed summary of the S2-scenes of the 2018 vegetation period used for classification. Due the BR *Wienerwald* is in the overlapping area of two orbits, the amount of available image material is higher as usual.

| S2-Satellite	Date	Orbit	Sun Zenith Angle	Sun Azimuth Angle
B	08.04.2018	79	43.02	157.29
B	21.04.2018	122	37.72	160.39
A	06.05.2018	122	33.06	159.37
A	02.07.2018	79	28.23	147.73
B	09.08.2018	122	34.38	155.97
A	21.08.2018	79	38.49	154.81
B	29.08.2018	122	40.40	160.44
A	13.09.2018	122	45.59	163.93
B	18.09.2018	122	47.41	164.98
B	28.09.2018	122	51.10	166.96
A	30.09.2018	79	52.25	164.21
B	05.10.2018	79	54.08	165.12
A	10.10.2018	79	55.90	165.94
A	30.10.2018	79	62.82	168.14

Table 7 shows the confusion matrix based on the OBB-results of the tree species classification. The model achieved an overall accuracy of 83.2% for the 12 tree species. In general, conifers were better classified by the model than deciduous trees, with *Picea abies* (PA = 94.1%, UA = 93.4%) and *Pinus nigra* (PA = 93.0%, UA = 93.0%) were separated best. The worst result among the conifers was achieved for *Larix decidua* (PA = 72.0%, UA = 80.0%).

The main tree species of this region, *Fagus sylvatica* (PA = 90.7%, UA = 75.1%) achieved the best classification result among all deciduous trees, which can be explained partly by the high sample size used to train the model, but also *Alnus glutinosa* (PA = 80.8%, UA = 85.7%) as well as *Quercus spp.* (PA = 84.4%, UA = 84.8%) reached good results. The predict of the tree species, merged with the land cover map of chapter two, can be seen in Figure 11.

Table 7: Confusion matrix based on the OOB-result of the tree species model considering 7 broadleaved and 5 needleleaved tree species for the BR *Wienerwald* (UA: user's accuracy, PA: producer's accuracy, OA: overall accuracy).

BRWW - S2 - Tree Species	FS	AG	FE	QU	PR	CB	AC	PA	PN	PS	LD	PM	UA
Fagus sylvatica (FS)	272	4	10	26	5	22	15	0	2	0	6	0	75.1%
Alnus glutinosa (AG)	1	42	3	1	1	1	0	0	0	0	0	0	85.7%
Fraxinus excelsior (FE)	6	2	64	5	2	4	3	0	2	0	2	0	71.1%
Quercus sp. (QU)	13	1	7	195	5	4	4	0	0	0	1	0	84.8%
Prunus sp. (PR)	0	0	0	0	12	0	0	0	0	0	0	0	100.0%
Carpinus betulus (CB)	3	2	1	1	0	40	1	0	0	0	0	0	83.3%
Acer sp. (AC)	5	1	0	1	0	0	30	0	0	0	0	0	81.1%
Picea abies (PA)	0	0	0	0	0	0	0	127	1	4	1	3	93.4%
Pinus nigra (PN)	0	0	0	0	0	0	2	3	133	1	1	1	94.3%
Pinus sylvestris (PS)	0	0	0	0	0	0	0	3	3	72	3	5	83.7%
Larix decidua (LD)	0	0	2	1	0	0	0	0	2	2	36	2	80.0%
Pseudotsuga menziesii (PM)	0	0	0	0	0	0	0	2	0	0	0	45	95.7%
PA	90.7%	80.8%	73.6%	84.8%	48.0%	56.3%	54.5%	94.1%	93.0%	91.1%	72.0%	80.4%	
									$\varkappa$ =	0.806		**OA =**	**83.2%**

The parameters used for the Sentinel-1-classification are listed in Table 8. The pre-processed data was available via the Austrian Data Cube (EODC GmbH, 2020). For the classification Backscatter averages and ratios from VH and VV polarizations for leave-off and leave-on conditions were used. In addition, several phenological parameters such as start-of-season were obtained from the time series data.

Table 8: Summary of the Sentinel-1-parameters for the BR *Wienerwald* used for classification provided by the TU Vienna.

Parameter name	Parameter description
20180314_20180326_VH	Temporally averaged backscatter for leaf of period, VH
20180314_20180326_VV	Temporally averaged backscatter for leaf of period, VV
20180618_20180630_CPR	Temporally averaged backscatter for leaf on period, CPR
20180618_20180630_VH	Temporally averaged backscatter for leaf on period, VH
20180618_20180630_VV	Temporally averaged backscatter for leaf on period, VV
Rat_Leaf_on_of	Backscatter ratio between leaf on and leaf of conditions
eos_doy	End of season – day of year
los_days	Length of season in days
sos_doy	Start of season – day of year
HPAR-C1_2018_VH_A073	HPAR, C1 cosine parameter, VH, ascending orbit 73
HPAR-C1_2018_VH_D022	HPAR, C1 cosine parameter, VH, descending orbit 22
HPAR-C1_2018_VV_A073	HPAR, C1 cosine parameter, VV, ascending orbit 73
HPAR-C1_2018_VV_D022	HPAR, C1 cosine parameter, VV, descending orbit 22
HPAR-C2_2018_VH_A073	HPAR, C2 cosine parameter, VH, ascending orbit 73
HPAR-C2_2018_VH_D022	HPAR, C2 cosine parameter, VH, descending orbit 22
HPAR-C2_2018_VV_A073	HPAR, C2 cosine parameter, VV, ascending orbit 73
HPAR-C2_2018_VV_D022	HPAR, C2 cosine parameter, VV, descending orbit 22
HPAR-C3_2018_VH_A073	HPAR, C3 cosine parameter, VH, ascending orbit 73
HPAR-C3_2018_VH_D022	HPAR, C3 cosine parameter, VH, descending orbit 22
HPAR-C3_2018_VV_A073	HPAR, C3 cosine parameter, VV, ascending orbit 73
HPAR-C3_2018_VV_D022	HPAR, C3 cosine parameter, VV, descending orbit 22
HPAR-M0_2018_VH_A073	HPAR, temporal average, VH, ascending orbit 73
HPAR-M0_2018_VH_D022	HPAR, temporal average, VH, descending orbit 22
HPAR-M0_2018_VV_A073	HPAR, temporal average, VV, ascending orbit 73
HPAR-M0_2018_VV_D022	HPAR, temporal average, VV, descending orbit 22
HPAR-S1_2018_VH_A073	HPAR, S1 sine parameter, VH, ascending orbit 73
HPAR-S1_2018_VH_D022	HPAR, S1 sine parameter, VH, descending orbit 22
HPAR-S1_2018_VV_A073	HPAR, S1 sine parameter, VV, ascending orbit 73
HPAR-S1_2018_VV_D022	HPAR, S1 sine parameter, VV, descending orbit 22
HPAR-S2_2018_VH_A073	HPAR, S2 sine parameter, VH, ascending orbit 73
HPAR-S2_2018_VH_D022	HPAR, S2 sine parameter, VH, descending orbit 22
HPAR-S2_2018_VV_A073	HPAR, S2 sine parameter, VV, ascending orbit 73
HPAR-S2_2018_VV_D022	HPAR, S2 sine parameter, VV, descending orbit 22
HPAR-S3_2018_VH_A073	HPAR, S3 sine parameter, VH, ascending orbit 73
HPAR-S3_2018_VH_D022	HPAR, S3 sine parameter, VH, descending orbit 22
HPAR-S3_2018_VV_A073	HPAR, S3 sine parameter, VV, ascending orbit 73
HPAR-S3_2018_VV_D022	HPAR, S3 sine parameter, VV, descending orbit 22
HPAR-STD_2018_VH_A073	HPAR, model standard deviation, VH, ascending orbit 73
HPAR-STD_2018_VH_D022	HPAR, model standard deviation, VH, descending orbit 22
HPAR-STD_2018_VV_A073	HPAR, model standard deviation, VV, ascending orbit 73
HPAR-STD_2018_VV_D022	HPAR, model standard deviation, VV, descending orbit 22

The classification results for the model using only Sentinel-1 input data is shown in Table 9. The separation between coniferous and broadleaved trees works quite well, also the class-specific accuracies for the coniferous but also for *Fagus sylvatica* and *Quercus spp.* are quite good. Nevertheless, the overall accuracy of the Sentinel-1 based classification was not able to come close to the Sentinel-2-based classifications.

The combination of Sentinel-1 and Sentinel-2 data in Table 10 shows slightly improvements compared to the Sentinel-2 only result. The overall accuracy is around 0.5 percentage points higher.

Table 9: Confusion matrix based on the OOB-result for 7 broadleaved and 5 coniferous tree species of the BR *Wienerwald* using Sentinel-1 data (UA: user's accuracy, PA: producer's accuracy, OA: overall accuracy)

BRWW – S1 - Tree Species													
	FS	AG	FE	QU	PR	CB	AC	PA	PN	PS	LD	PM	UA
Fagus sylvatica (FS)	**236**	33	36	86	16	39	34	0	10	4	14	0	46.5%
Alnus glutinosa (AG)	0	**0**	0	1	0	1	0	0	0	0	0	1	NA
Fraxinus excelsior (FE)	3	2	**6**	2	1	1	4	0	0	0	0	0	31.6%
Quercus sp. (QU)	47	14	40	**140**	2	18	13	0	4	1	0	0	50.2%
Prunus sp. (PR)	1	0	0	0	**1**	0	0	0	0	0	0	0	50.0%
Carpinus betulus (CB)	0	0	2	0	0	**4**	0	1	0	0	0	1	50.0%
Acer sp. (AC)	0	0	0	0	0	0	**0**	0	0	0	0	0	NA
Picea abies (PA)	1	0	0	0	0	2	0	**119**	2	7	0	24	76.8%
Pinus nigra (PN)	7	2	2	1	0	5	2	1	**114**	19	1	5	71.7%
Pinus sylvestris (PS)	0	0	0	0	1	0	0	5	11	**44**	1	5	65.7%
Larix decidua (LD)	5	1	1	0	4	1	2	1	0	2	**31**	1	63.3%
Pseudotsuga menziesii (PM)	0	0	0	0	0	0	0	8	2	2	3	**19**	55.9%
PA	78.7%	0.0%	6.9%	60.9%	4.0%	5.6%	0.0%	88.1%	79.7%	55.7%	62.0%	33.9%	
										ϰ = 0.469		OA =	**55.7%**

Table 10: Confusion matrix based on the OOB-result for 7 broadleaved and 5 coniferous tree species of the BR *Wienerwald* using Sentinel-1 and Sentinel-2 data together (UA: user's accuracy, PA: producer's accuracy, OA: overall accuracy)

BRWW – S1+S2 - Tree Species													
	FS	AG	FE	QU	PR	CB	AC	PA	PN	PS	LD	PM	UA
Fagus sylvatica (FS)	**271**	2	9	28	8	19	16	0	1	0	3	0	75.9%
Alnus glutinosa (AG)	0	**43**	1	0	0	1	0	0	0	0	0	0	95.6%
Fraxinus excelsior (FE)	6	2	**64**	6	0	3	4	0	1	0	2	0	72.7%
Quercus sp. (QU)	16	1	9	**193**	6	4	3	0	0	0	0	0	83.2%
Prunus sp. (PR)	0	0	0	0	**10**	0	0	0	0	0	0	0	100%
Carpinus betulus (CB)	2	3	3	2	0	**44**	1	0	1	0	0	0	78.6%
Acer sp. (AC)	4	1	0	0	1	0	**29**	0	0	0	0	0	82.9%
Picea abies (PA)	0	0	0	0	0	0	0	**129**	1	4	1	5	92.1%
Pinus nigra (PN)	1	0	0	0	0	0	2	3	**135**	2	2	0	93.1%
Pinus sylvestris (PS)	0	0	0	0	0	0	0	2	3	**70**	2	3	87.5%
Larix decidua (LD)	0	0	1	1	0	0	0	0	1	3	**40**	2	83.3%
Pseudotsuga menziesii (PM)	0	0	0	0	0	0	0	1	0	0	0	**46**	97.9%
PA	90.3%	82.7%	73.6%	83.9%	40.0%	62.0%	52.7%	95.6%	94.4%	88.6%	80.0%	82.1%	
										ϰ = 0.811		OA =	**83.7%**
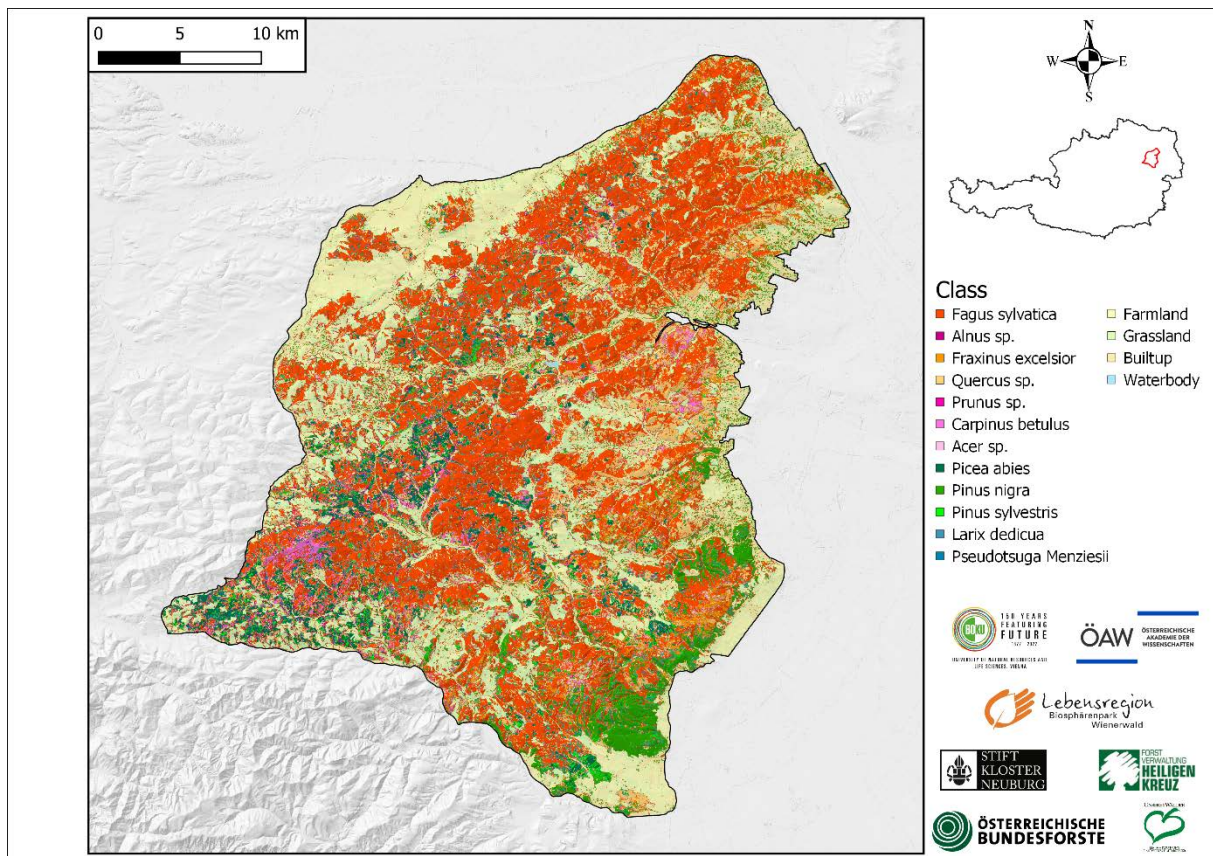
Figure 11: Tree species map of the BR *Wienerwald* containing detailed information of 7 broadleaved as well as 5 coniferous tree-species, based on Sentinel-2-imagery

Using the Sentinel-2 tree species classification, a Biodiversity map was calculated for the BR *Wienerwald*. For this, a pixel-based Shannon-Index-calculation was applied on the raster image using following formula:

Shannon index (H')	$-\sum p_i \ln(p_i)$	$[0, \ln(S)]$	The Shannon-Index expresses the frequency of the ith species in a community

The relative biodiversity-range is between 0 and 2.197 for each individual pixel, whereby higher values indicate higher tree species diversity. Looking on the biodiversity-map in Figure 12, it is noticeable that tree species biodiversity shows a north-south gradient and a west-east gradient, with the south-west presenting the highest values.

In addition, a map of spectral species was calculated by BR *Wienerwald*, which is shown in Figure 13. This concept by Féret and Asner (2014) assumes that species can be distinguished purely based on their spectral signature. However, the spectral species do not necessarily have to represent biological species.

Figure 12: Biodiversity-Shannon-Index calculated for each individual pixel, based on the tree species map of the BR *Wienerwald*. Higher values indicate higher tree species biodiversity
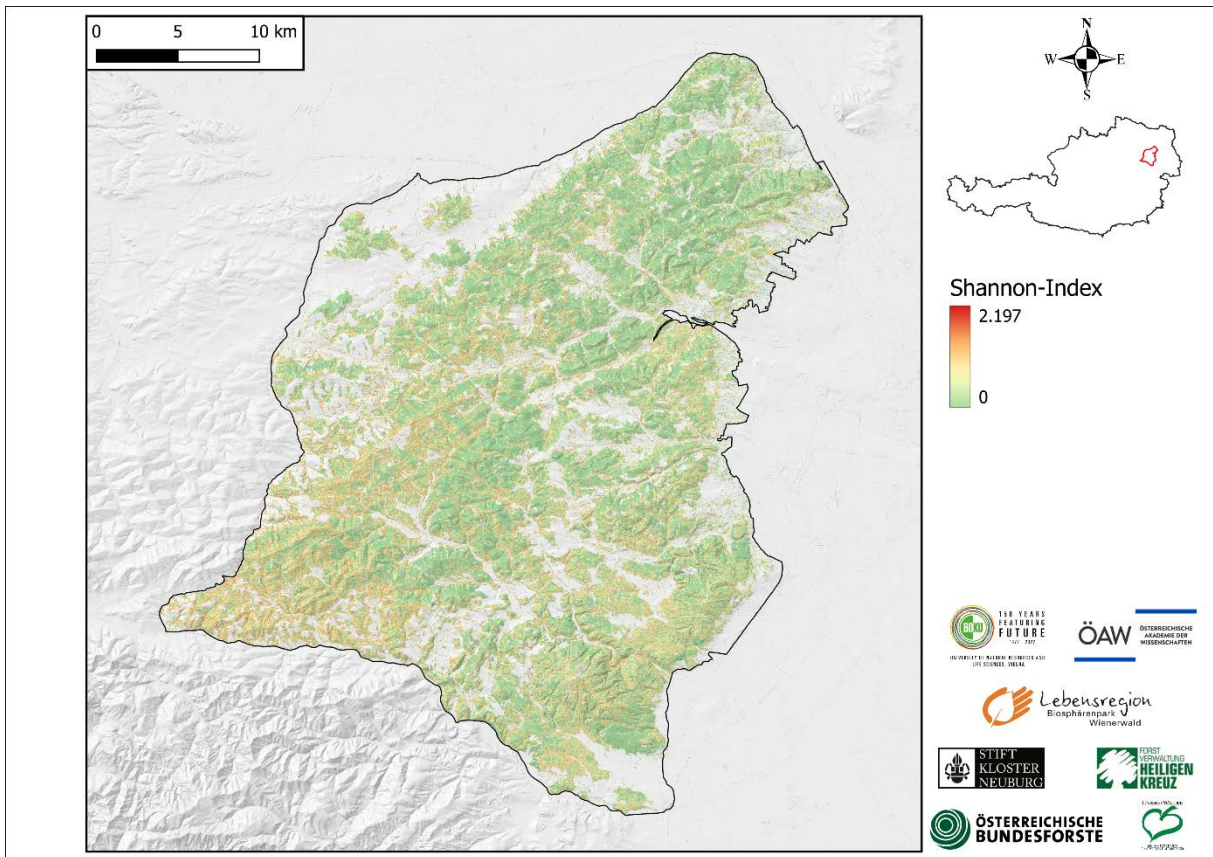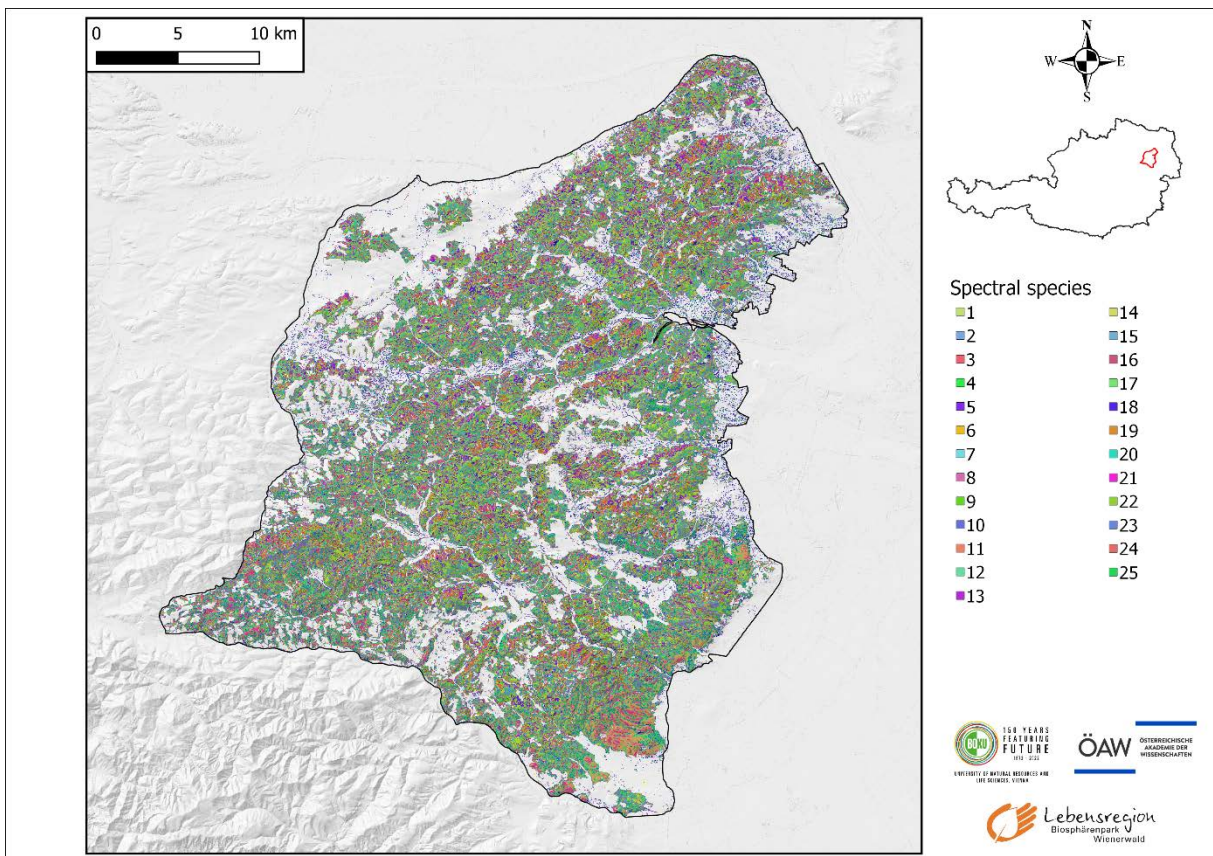

Figure 13: Spectral species map based on Sentienl-2 scenes of the year 2018

4. Analysis of grasslands in BR *Wienerwald* (WP 4)

The reference polygons ("Offenlandkartierung") were provided by the BR *Wienerwald*. First, an attempt was made to separate the main classes with a focus on the open land using classification algorithms. For this purpose, the same Sentinel-2 scenes as for the tree species classification were used and again one pixel from each polygon was used for training.

The achieved classification result shown in Table 11 shows some potential for the separation of these broad classes. However, the class-specific accuracies are not satisfying. The reasons for this are the similarity of some classes but especially the spatially small extent of some classes which do not always fit with the 10 or 20 m pixels of Sentinel-2. A further reduction of the reference data in terms of size or more intensive matching with higher resolution data, as was done for the tree species reference data set, could at least provide some improvement. Also, a restriction to fewer but possibly more relevant classes could be considered.

Table 11: Confusion matrix based on the OOB-result for broad classes of the open land mapping of the BR *Wienerwald* using Sentinel-2 data (UA: user's accuracy, PA: producer's accuracy, OA: overall accuracy)

	AWG	BRS	BS	FGR	GHFG	GGH	NAG	NRG	NFSA	NR	OG	TT	W	UA
Äcker & Weingärten (AWG)	**722**	144	107	16	55	39	41	70	10	61	61	0	5	54.2%
Böschungen, Raine & Säume (BRS)	15	**61**	19	8	17	8	3	6	3	12	10	2	1	37.0%
Bauland und Siedlung (BS)	23	107	**476**	22	80	139	46	39	30	42	100	7	17	42.2%
Feucht-Grünland & Röhrichte (GHFG)	11	12	7	**187**	17	17	58	53	5	18	21	1	14	44.4%
Gebüsche, Hecken, Feldgehölze, Grabenwälder (GHFG)	13	61	67	34	**437**	184	60	31	13	39	93	10	87	38.7%
Gewässerbegleitende Gehölze & Hochstaudenfluren (GGH)	1	16	47	17	77	**146**	11	12	2	5	30	11	18	37.2%
Nährstoffarmes Grünland (NAG)	60	44	45	102	48	18	**466**	163	14	49	65	0	20	42.6%
Nährstoffreiches Grünland (NRG)	113	46	50	175	45	52	187	**528**	0	30	131	0	4	38.8%
Natürliche Fels- & Steinbildungen, Abbauflächen (NFSA)	0	0	0	0	0	0	1	0	**7**	0	0	0	1	77.8%
Neophyten- & Ruderalbestände (NR)	0	1	0	0	0	0	0	0	0	**1**	0	0	0	50.0%
Obstbestände & sonstige Gehölzanpflanzungen (OG)	41	48	132	33	103	98	65	89	3	23	**461**	2	17	41.3%
Teiche & Tümpel (TT)	0	1	3	0	2	4	1	0	2	0	0	**61**	0	82.4%
Wald (W)	1	6	47	32	119	65	61	9	7	25	28	8	**816**	66.7%
PA	72.2%	11.2%	47.6%	29.9%	43.7%	19.0%	46.6%	52.8%	7.3%	0.3%	46.1%	59.8%	81.6%	

| | | | | | | | | $\varkappa =$ | 0.469 | **OA =** | **55.7%** | | | |

The experiences of the FFG-project SatGrass (https://satgrass.at) highlighted that the amount of data acquired by Sentinel-2 alone is often not sufficient. This was also the case for the mowing analysis in the BR *Wienerwald* where the already presented data pool of cloud-free Sentinel-2 data was not enough to produce dense time series. Therefore, the cut detection was performed on the so-called Harmonized Sentinel-2 and Landsat-8 (HLS) data due to the dense time series it provides and space requirement. HLS data is delivered at 30 m resolution, which means some small farm plots may not be detectable. It was decided that the trade-off of coarser resolution for a denser time series and smaller storage space requirements was acceptable.

The used method was developed in the mentioned project SatGrass and applied to the polygons provided by the BR *Wienerwald* Management. Data was extracted at the plot (polygon) level for the years 2016, 2017, 2018, 2019, 2020 and 2021 and cut detection occurred between April 1st and November 15th for each year around the BR *Wienerwald*. The given shapefile contained polygons that could cover multiple grassland plots which could lead to missed cuts if one of the covered plots is in the processing growing while another is being cut. Each plot was shrunk by 10 meters (inner buffer) to account a little for the image 'wobbling' as the satellites do not extract images in the exact same spot every time. This also helps to ensure that only field values were being extracted, and not the boundaries of the farm plot which may have more than just vegetation on them. First, potentially cloudy timestamps were identified and removed from the valid observations. Second, a light data smoothing was applied, keeping most originally extracted values while removing potentially cloudy and shadowy days which escaped masking.

Mowing events, using the corrected valid observations, were then detected using methods to construct an idealized curve adapted from Griffiths in a similar project spanning the grasslands of Germany (Griffiths et al., 2020). An idealized growth curve was constructed by smoothing the actual valid NDVI and then iteratively smoothing the results of each smoothing iteration, including maximum values in each iteration so that the upper envelope is always being smoothed. Cuts were then detected as the difference between the idealized and actual growth curves. If this difference exceeded a -0.1 NDVI, a potential cut could be detected. Cuts could only be detected at timestamps which showed a negative net NDVI change. A binary classification model then checked each cut detection to ensure the detected cut was not a cloud which made it through the masking and preprocessing steps. If the detection was a cloud, it was removed from potential detections.

It is possible that multiple detections can occur per actual cut as grass is cut, dries, and is removed from the field if the time series is dense enough. This was accounted for by temporally masking out detections 28 days from the most recent detection while moving through the timeline.

The described cut detection method is a development by the Institute of Geomatics, University of Natural Resources and Life Sciences Vienna for the SatGrass project.

Figure 14 shows a visualization of the cut detection methods. These methods were trained using only a Sentinel-2 time series for the year 2021 on homogenously managed grasslands. The known cut detection day of June 13th was reported by independent analysts and its accuracy can be trusted. The time series depicts removed cloudy days and a false positive which may have skewed cut detection results if not detected. Note how in May and early June there are NDVI dips, but no detected cut in the final output. This is due to the model which looks at each detected potential cut deciding this was a cloudy day, and not a cut.
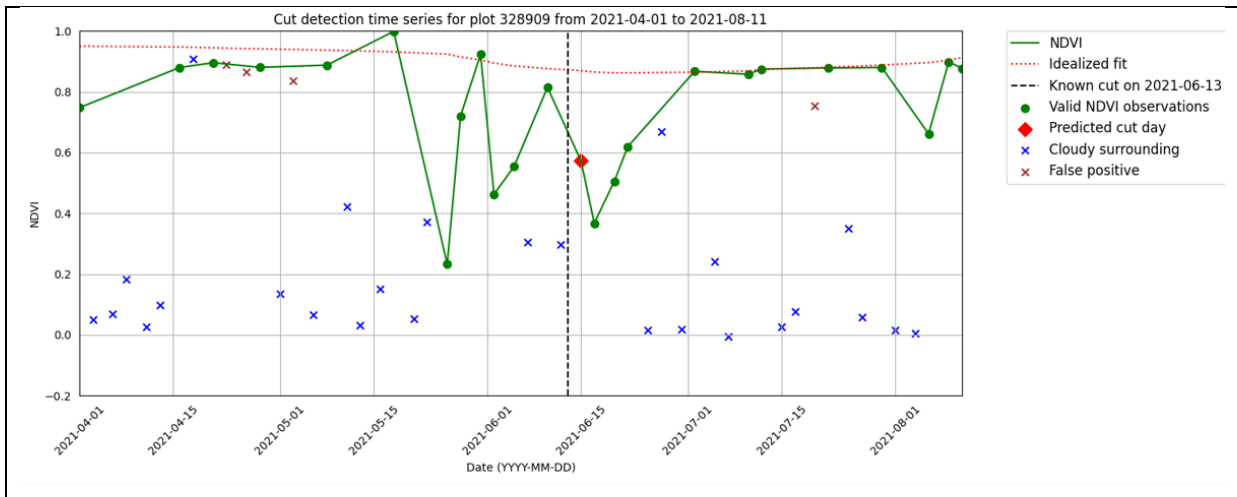
Figure 14: Example of cut detection with known cut dates (training data for developing the method for the satgrass project)

Grassland use intensity is then estimated by counting the number of cuts per season for each plot. The cuts per year were further averaged over the years and for all polygons larger than 0.1 ha. The plot in Figure 15 shows clear tendencies despite the large scattering within the classes. The intensively used classes ("*Intensivwiese*" and "*Glatthafer-Fettwiese*") show the highest number of cuts. Other classes ("*Fels-Trockenrasen*") are characterized by a very low number of cuts per year. Further analyses are planned in coordination with the BR *Wienerwald* Management to analyze differences between years and locations. Unfortunately, it was not possible to complete these analyses in the course of the project due to time constraints on the part of BR.

Figure 15: Cuts per year averaged for the period 2016-2020 for different open land classes provided by the BR *Wienerwald*

5. Historical developments of the land cover of all Austrian BRs (WP 5)

For the analysis of land cover changes the reference points were checked for different time steps. For the BR *Großes Walsertal* orthoimages for different time steps were available. For the other BRs the Landsat data were analyzed for changes and in addition, google earth images and web GIS sites of the federal s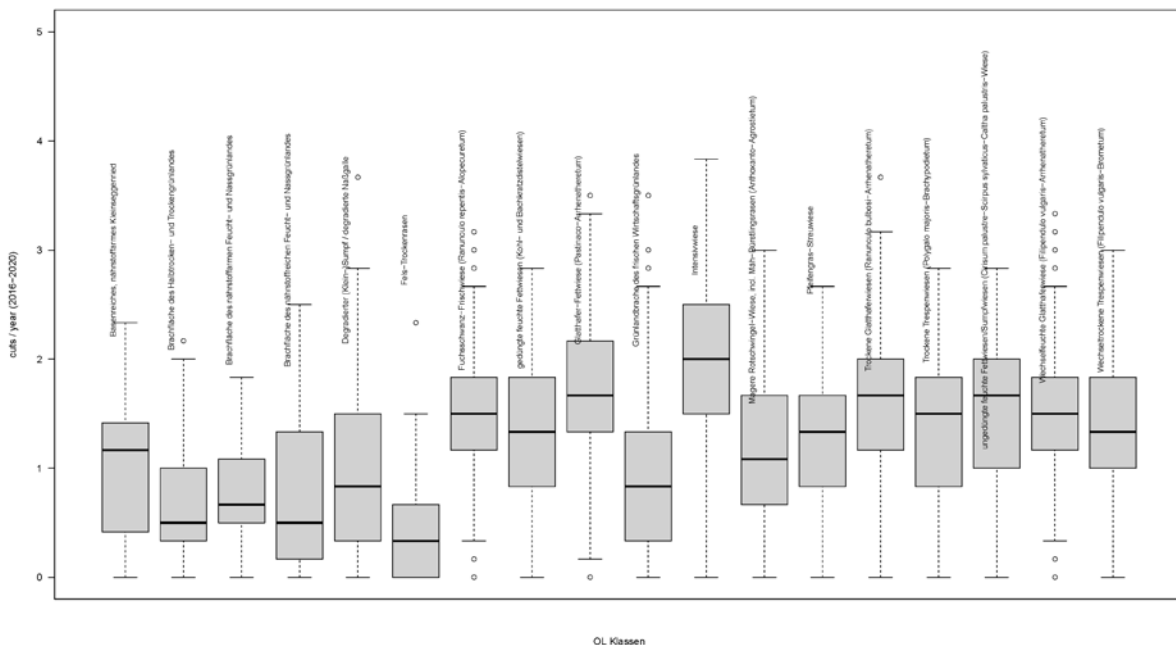tates were checked. The examples in Figure 16 highlights that changes were already observed on some reference points, which have to be considered for the model training.

Figure 16. Examples of changes in land cover from 199x, 2001 and 2018 (CIR composite orthoimages) on reference data points for the BR *Großes Walsertal*.

Using Landsat satellites, time series of land cover classes were created for all three biosphere reserves, with the period from 1984 to 2018 divided into four time-intervals / periods (Table 12 - Table 14).

Table 12: Overview of the Landsat-scenes (data pool) used for the BR *Wienerwald* historical land cover-classification for different periods.

BR *Wienerwald*			
1984-1992	1993-2004	2005-2011	2012-2018
LT05_L1TP_190026_19840805_20200918_02_T1	LE07_L1TP_190026_20000910_20200917_02_T1	LT05_L1GS_190026_20111003_20200820_02_T2	LC08_L1TP_190026_20130415_20200912_02_T1
LT05_L1TP_190026_19850824_20200918_02_T1	LE07_L1TP_190026_20010524_20200917_02_T1	LT05_L1TP_190026_20050527_20200902_02_T1	LC08_L1TP_190026_20130618_20200912_02_T1
LT05_L1TP_190026_19860624_20201008_02_T1	LE07_L1TP_190026_20030327_20200915_02_T1	LT05_L1TP_190026_20050730_20200902_02_T1	LC08_L1TP_190026_20130805_20200912_02_T1
LT05_L1TP_190026_19870510_20201014_02_T1	LT05_L1TP_190026_19930424_20200914_02_T1	LT05_L1TP_190026_20060615_20200901_02_T1	LC08_L1TP_190026_20130906_20200912_02_T1
LT05_L1TP_190026_19880426_20200917_02_T1	LT05_L1TP_190026_19930814_20200913_02_T1	LT05_L1TP_190026_20070720_20200830_02_T1	LC08_L1TP_190026_20150320_20200909_02_T1
LT05_L1TP_190026_19880731_20200917_02_T1	LT05_L1TP_190026_19950905_20200912_02_T1	LT05_L1TP_190026_20100407_20200824_02_T1	LC08_L1TP_190026_20160914_20200906_02_T1
LT05_L1TP_190026_19890328_20200916_02_T1	LT05_L1TP_190026_19951023_20200912_02_T1	LT05_L1TP_190026_20110629_20200822_02_T1	LC08_L1TP_190026_20160930_20200906_02_T1
LT05_L1TP_190026_19910910_20200915_02_T1	LT05_L1TP_190026_19961025_20200911_02_T1		LC08_L1TP_190026_20170410_20200904_02_T1
LT05_L1TP_190026_19911028_20200915_02_T1	LT05_L1TP_190026_19970403_20200910_02_T1		LC08_L1TP_190026_20170528_20200903_02_T1
LT05_L1TP_190026_19921014_20200914_02_T1	LT05_L1TP_190026_19970825_20200910_02_T1		LC08_L1TP_190026_20170613_20200903_02_T1
	LT05_L1TP_190026_19980508_20200909_02_T1		LC08_L1TP_190026_20181006_20200830_02_T1
	LT05_L1TP_190026_19980812_20200908_02_T1		
	LT05_L1TP_190026_19991018_20200907_02_T1		
	LT05_L1TP_190026_20000513_20200907_02_T1		
	LT05_L1TP_190026_20010430_20200906_02_T1		
	LT05_L1TP_190026_20010820_20200906_02_T1		
	LT05_L1TP_190026_20020620_20200905_02_T1		
	LT05_L1TP_190026_20030810_20200904_02_T1		

Table 13: Overview of the Landsat-scenes (data pool) used for the BR *Großes Walsertal* historical land cover-classification for different periods.

BR *Großes Walsertal*			
1984-1992	1993-2004	2005-2011	2012-2018
LT05_L1TP_193027_19850728_20200918_02_T1	LE07_L1TP_193027_19990913_20200918_02_T1	LT05_L1TP_193027_20061010_20200831_02_T1	LC08_L1TP_193027_20200728_20200908_02_T1
LT05_L1TP_193027_19850813_20200918_02_T1	LT05_L1TP_193027_19970915_20200909_02_T1	LT05_L1TP_193027_20061026_20200831_02_T1	LC08_L1TP_193027_20200914_20200919_02_T1
LT05_L1TP_193027_19880720_20200917_02_T1	LT05_L1TP_193027_19990703_20200908_02_T1	LT05_L1TP_193027_20090815_20200827_02_T1	LC08_L1TP_194027_20140703_20200911_02_T1
LT05_L1TP_193027_19891027_20200916_02_T1	LT05_L1TP_193027_20000619_20200906_02_T1	LT05_L1TP_193027_20090831_20200825_02_T1	LC08_L1TP_194027_20140719_20200911_02_T1
LT05_L1TP_193027_19900928_20200915_02_T1	LT05_L1TP_193027_20010825_20200906_02_T1	LT05_L1TP_193027_20110704_20200822_02_T1	LC08_L1TP_194027_20171015_20200902_02_T1
LT05_L1TP_193027_19901014_20200915_02_T1	LT05_L1TP_193027_20030916_20200904_02_T1	LT05_L1TP_193027_20110906_20200820_02_T1	
LT05_L1TP_193027_19910729_20200915_02_T1	LT05_L1TP_193027_20040630_20200903_02_T1	LT05_L1TP_194027_20090721_20200827_02_T1	
LT05_L1TP_193027_19910830_20200915_02_T1	LT05_L1TP_193027_20040902_20200903_02_T1	LT05_L1TP_194027_20100708_20200823_02_T1	
LT05_L1TP_193027_19920816_20200914_02_T1	LT05_L1TP_193027_20040918_20200903_02_T1		
LT05_L1TP_193027_19920917_20200914_02_T1	LT05_L1TP_194027_19980808_20200908_02_T1		
LT05_L1TP_194027_19910821_20200915_02_T1	LT05_L1TP_194027_19980909_20200908_02_T2		
	LT05_L1TP_194027_19990912_20200907_02_T1		
	LT05_L1TP_194027_20010731_20200906_02_T1		
	LT05_L1TP_194027_20040909_20200903_02_T1		

Table 14: Overview of the Landsat-scenes (data pool) used for the BRs *Salzburger Lungau* and *Kärntner Nockberge* historical land cover-classification for different periods.

BRs *Salzburger Lungau* and *Kärntner Nockberge*			
1984-1992	1993-2004	2005-2011	2012-2018
LT05_L1TP_191027_19841031_20200918_02_T1	LE07_L1TP_191027_20020603_20200916_02_T1	LE07_L1TP_191027_20050729_20200914_02_T1	LC08_L1TP_191027_20180927_20200830_02_T1
LT05_L1TP_191027_19851018_20200918_02_T1	LE07_L1TP_191027_20020721_20200916_02_T1	LE07_L1TP_191027_20070719_20200913_02_T1	LE07_L1TP_191027_20120630_20200909_02_T1
LT05_L1TP_191027_19860903_20200918_02_T1	LE07_L1TP_191027_20030926_20200915_02_T1	LE07_L1TP_191027_20110628_20200910_02_T1	LE07_L1TP_191027_20120918_20200908_02_T1
LT05_L1TP_191027_19870922_20201014_02_T1	LT05_L1GS_191027_20041006_20200903_02_T2	LE07_L1TP_191027_20111002_20200909_02_T1	LE07_L1TP_191027_20140924_20200905_02_T1
LT05_L1TP_191027_19880807_20200917_02_T1	LT05_L1TP_191027_19940723_20200913_02_T1	LE07_L1TP_191027_20111018_20200909_02_T1	LE07_L1TP_191027_20141010_20200905_02_T1
LT05_L1TP_191027_19900712_20200915_02_T1	LT05_L1TP_191027_19960930_20200911_02_T1	LT05_L1TP_191027_20050619_20200902_02_T1	LE07_L1TP_191027_20170831_20200830_02_T1
LT05_L1TP_191027_19900914_20200915_02_T1	LT05_L1TP_191027_19970629_20200910_02_T1	LT05_L1TP_191027_20060910_20200831_02_T1	LE07_L1TP_191027_20181005_20200828_02_T1
LT05_L1TP_191027_19900930_20200915_02_T1	LT05_L1TP_191027_19970901_20200909_02_T1	LT05_L1TP_191027_20061012_20200831_02_T1	
LT05_L1TP_191027_19901016_20200915_02_T1	LT05_L1TP_191027_19970917_20200910_02_T1	LT05_L1TP_191027_20090614_20200827_02_T1	
LT05_L1TP_191027_19920818_20200914_02_T1	LT05_L1TP_191027_20000909_20200907_02_T1	LT05_L1TP_191027_20091004_20200825_02_T1	
	LT05_L1TP_191027_20030918_20200904_02_T1	LT05_L1TP_191027_20100921_20200823_02_T1	
	LT05_L1TP_191027_20040819_20200903_02_T1	LT05_L1TP_191027_20110823_20200820_02_T1	

The overall accuracies of the land cover classifications for the BR *Wienerwald* range between 83.4% and 92.1% (Table 15). For all biosphere reserves, the lowest classification accuracies are found in the longest dated time intervals 1984-1992, for which only Landsat 5 satellite images were used. The younger the time interval, the more a trend towards increased accuracy becomes apparent. This can be attributed to a better quality of the data and a higher spectral resolution of the Landsat-7 and Landsat-8-satellites. Both have an additional panchromatic channel, which records in a wavelength range of 0.515 μm to 0.896 μm and 0.503 μm to 0.676 μm, respectively, with a spatial resolution of 15 m. The higher the spectral resolution, the more accurate the data in general. The best result from the last period is also only slightly worse than the land cover classification result based on Sentinel-2 data (Chapter 2).

Table 15: Confusion matrix based on the OOB-result of the BR *Wienerwald* land cover classification using Landsat-imagery for the periods 1984-1992, 1993-2004, 2005-2011 and 2012-2018 (UA: user's accuracy, PA: producer's accuracy, OA: overall accuracy).

BRWW - LS	1984-1992						
	farmland	grassland	built-up	waterbody	broadleaved	needleleaved	UA
farmland	**66**	13	5	0	2	1	75.9%
grassland	8	**64**	6	0	9	3	71.1%
built-up	2	4	**94**	1	7	0	87.0%
waterbody	0	0	0	**12**	0	0	100%
broadleaved	0	16	2	1	**350**	28	88.2%
needleleaved	0	6	0	0	16	**65**	74.7%
PA	86.8%	62.1%	87.9%	85.7%	91.1%	67.0%	
				ϰ =	0.759	OA =	83.4%

BRWW - LS	1993-2004						
	farmland	grassland	built-up	waterbody	broadleaved	needleleaved	UA
farmland	**65**	8	3	1	3	0	81.2%
grassland	10	**73**	1	0	8	1	78.5%
built-up	0	6	**100**	1	3	1	90.1%
waterbody	0	0	0	**12**	0	0	100%
broadleaved	1	15	3	0	**363**	12	92.1%
needleleaved	0	1	0	0	7	**83**	91.2%
PA	85.5%	70.9%	93.5%	85.7%	94.5%	85.6%	
				ϰ =	0.843	OA =	89.1%

BRWW - LS	2005-2011						
	farmland	grassland	built-up	waterbody	broadleaved	needleleaved	UA
farmland	**58**	5	2	0	2	1	85.3%
grassland	12	**79**	2	0	3	1	81.4%
built-up	3	6	**101**	2	2	0	88.6%
waterbody	0	0	0	**12**	0	0	100%
broadleaved	2	10	2	0	**368**	13	93.2%
needleleaved	1	3	0	0	9	**82**	86.3%
PA	76.3%	76.7%	94.4%	85.7%	95.8%	84.5%	
				ϰ =	0.850	OA =	89.6%

BRWW - LS	2012-2018						
	farmland	grassland	built-up	waterbody	broadleaved	needleleaved	UA
farmland	**69**	7	2	0	0	0	88.5%
grassland	5	**81**	0	0	7	0	87.1%
built-up	2	5	**103**	0	3	1	90.4%
waterbody	0	0	0	**14**	0	0	100%
broadleaved	0	8	2	0	**367**	11	94.6%
needleleaved	0	2	0	0	7	**85**	90.4%
PA	90.8%	78.6%	96.3%	100%	95.6%	87.6%	
				ϰ =	0.886	OA =	92.1%

At first glance, the maps shown in Figure 17 suggest that the class distribution is all too different. However, detailed analyses show that small-scale changes are definitely discernible.
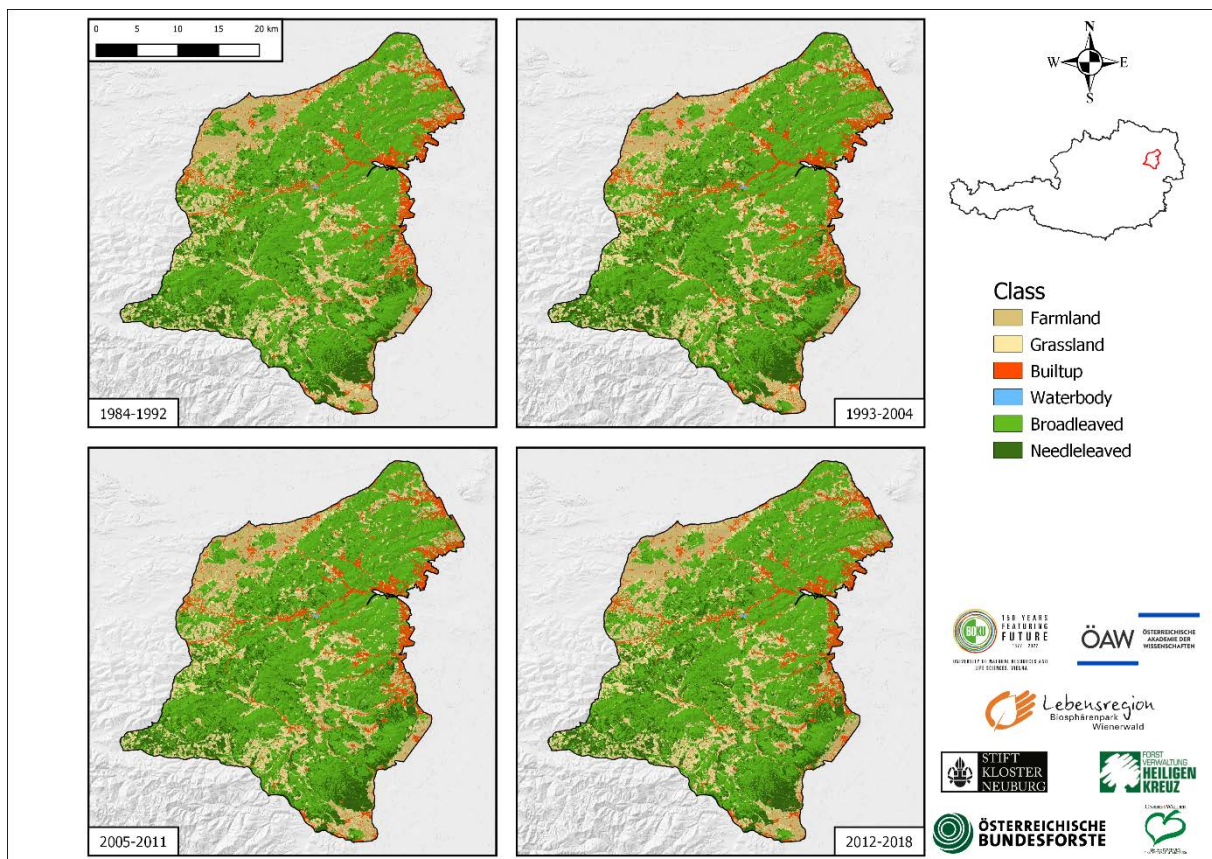
Figure 17: Historical land cover maps of the BR *Wienerwald* based on Landsat-imagery for the periods 1984-1992, 1993-2004, 2005-2011 and 2012-2018

The confusion matrices in Table 16 show the OOB-results of the historical Landsat-models of the *BR Großes Walsertal*. The best overall accuracy of 88.5 % was achieved in the period 2011-2018, while the results of the various periods show the same decreasing trend in OA the older the periods are. Although most classes achieved good results for both, Producer's and User's accuracy, the classes mixed and broadleaved couldn't be separated satisfying. This might be explained due to the lack of samples in the coniferous dominated ecosystem.

Table 16: Confusion matrix based on the OOB-result of the BR *Großes Walsertal* land cover classification using Landsat-imagery for the periods 1984-1992, 1993-2004, 2005-2011 and 2012-2018 (UA: user's accuracy, PA: producer's accuracy, OA: overall accuracy).

BRGWT - LS	1984-1992							
	grassland	built-up	rock	waterbody	broadleaved	mixed	needleleaved	UA
grassland	**274**	5	3	0	6	1	12	91.0%
built-up	1	**55**	2	0	0	0	0	94.8%
rock	1	2	**99**	2	0	0	1	94.3%
waterbody	0	0	0	**10**	0	0	0	100%
broadleaved	1	0	0	0	**32**	13	1	68.1%
mixed	2	0	0	0	13	**44**	14	60.3%
needleleaved	3	0	0	1	2	25	**89**	74.2%
PA	97.2%	88.7%	95.2%	76.9%	60.4%	53.0%	76.1%	
						$\varkappa =$ 0.796	**OA =**	**84.5%**

BRGWT - LS	1993-2004							
	grassland	built-up	rock	waterbody	broadleaved	mixed	needleleaved	UA
grassland	**268**	6	2	1	3	0	5	94.0%
built-up	1	**55**	1	0	0	0	0	96.5%
rock	3	1	**101**	1	0	0	0	95.3%
waterbody	0	0	0	**11**	0	0	0	100%
broadleaved	1	0	0	0	**39**	14	1	70.9%
mixed	3	0	0	0	10	**44**	14	62.0%
needleleaved	6	0	0	0	1	25	**97**	75.2%
PA	95.0%	88.7%	97.1%	84.6%	73.6%	53.0%	82.9%	
						$\varkappa =$ 0.819	**OA =**	**86.1%**

BRGWT - LS	2005-2011							
	grassland	built-up	rock	waterbody	broadleaved	mixed	needleleaved	UA
grassland	**272**	4	2	0	3	1	5	94.8%
built-up	1	**57**	1	0	0	0	0	96.6%
rock	3	1	**101**	0	0	0	0	96.2%
waterbody	0	0	0	**13**	0	0	0	100%
broadleaved	0	0	0	0	**40**	16	0	71.4%
mixed	3	0	0	0	10	**42**	15	60.0%
needleleaved	3	0	0	0	0	24	**97**	78.2%
PA	96.5%	91.9%	97.1%	100%	75.5%	50.6%	82.9%	
						$\varkappa =$ 0.832	**OA =**	**87.1%**

BRGWT - LS	2012-2018							
	grassland	built-up	rock	waterbody	broadleaved	mixed	needleleaved	UA
grassland	**274**	3	2	0	3	1	4	95.5%
built-up	1	**58**	2	0	0	0	0	95.1%
rock	1	1	**100**	0	0	0	0	98.0%
waterbody	0	0	0	**13**	0	0	0	100.0%
broadleaved	1	0	0	0	**38**	9	1	77.6%
mixed	1	0	0	0	11	**52**	15	65.8%
needleleaved	4	0	0	0	1	21	**97**	78.9%
PA	97.2%	93.5%	96.2%	100.0%	71.7%	62.7%	82.9%	
						$\varkappa =$ 0.850	**OA =**	**88.5%**

The historical land cover maps of the BR *Großes Walsertal* can be seen in Figure 18. While the BR is coniferous dominated, beroadleaved and mixed species can especially be found lower regions of the valleys. The rock class was often misclassified as a building, which can be explained on the one hand by the low number of samples, but above all by the spectral similarity of the classes.
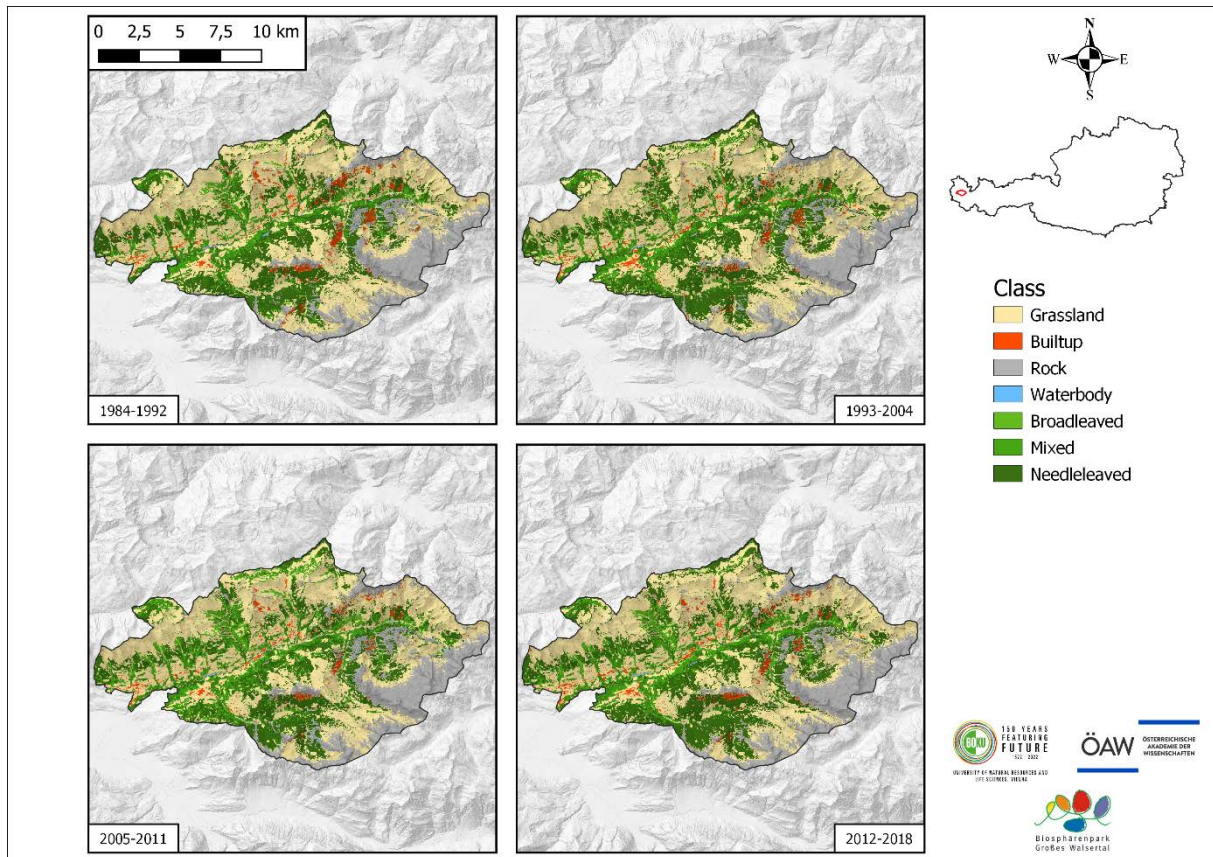

Figure 18: Historical land cover maps of the BR *Großes Walsertal* based on Landsat-imagery

In the OOB results of the BRs *Salzburger Lungau* and *Kärntner Nockberge*, the trend that younger periods produce better results is also evident, as in the case of the other two BRs. However, the best result was achieved by period 2005-2011 with OA = 91.7 %, the worst by period 1984-1992 with OA = 85.5 %. Similar to BR *Großes Walsertal*, the deciduous and mixed forest classes, which are represented with fewer samples, also achieved the lowest results. In particular, the class dwarf pine, which was very often classified as coniferous forest, stands out. Since the dwarf pine itself is also a coniferous forest species, this confusion seems obvious.

Table 17: Confusion matrix based on the OOB-result of the BRs *Salzburger Lungau* and *Kärntner Nockberge* land cover classification using Landsat-imagery for the periods 1984-1992, 1993-2004, 2005-2011 and 2012-2018 (UA: user's accuracy, PA: producer's accuracy, OA: overall accuracy).

BRSLKN - LS	1984-1992								
	grassland	built-up	rock	waterbody	broadleaved	mixed	needleleaved	dwarf pine	UA
grassland	**411**	9	5	2	3	4	32	4	87.4%
built-up	0	**57**	0	1	1	1	0	0	95.0%
rock	3	1	**115**	1	1	0	0	0	95.0%
waterbody	0	0	1	**48**	0	0	0	0	98.0%
broadleaved	1	0	1	0	**16**	18	2	0	42.1%
mixed	3	0	0	0	35	**47**	7	1	50.5%
needleleaved	47	1	1	0	5	29	**687**	17	87.3%
dwarf pine	1	0	0	0	0	0	1	**25**	92.6%
PA	88.2%	83.8%	93.5%	92.3%	26.2%	47.5%	94.2%	53.2%	
						ϰ =	0.791	OA =	**85.5%**

BRSLKN - LS	1993-2004								
	grassland	built-up	rock	waterbody	broadleaved	mixed	needleleaved	dwarf pine	UA
grassland	**443**	4	2	0	3	3	17	3	93.3%
built-up	1	**61**	1	1	0	0	0	0	95.3%
rock	1	2	**117**	0	0	0	0	0	97.5%
waterbody	0	0	1	**50**	0	0	0	0	98.0%
broadleaved	0	0	0	0	**32**	19	0	0	62.7%
mixed	2	0	0	0	26	**59**	12	0	59.6%
needleleaved	19	1	2	1	0	18	**700**	13	92.8%
dwarf pine	0	0	0	0	0	0	0	**31**	100%
PA	95.1%	89.7%	95.1%	96.2%	52.5%	59.6%	96.0%	66.0%	
						ϰ =	0.868	OA =	**90.8%**

BRSLKN - LS	2005-2011								
	grassland	built-up	rock	waterbody	broadleaved	mixed	needleleaved	dwarf pine	UA
grassland	**453**	3	3	0	1	0	11	3	95.6%
built-up	0	**64**	0	1	0	0	0	0	98.5%
rock	1	1	**117**	1	0	0	0	0	97.5%
waterbody	0	0	1	**50**	0	0	0	0	98.0%
broadleaved	1	0	0	0	**29**	17	1	0	60.4%
mixed	0	0	0	0	28	**63**	7	0	64.3%
needleleaved	11	0	2	0	3	19	**709**	20	92.8%
dwarf pine	0	0	0	0	0	0	1	**24**	96.0%
PA	97.2%	94.1%	95.1%	96.2%	47.5%	63.6%	97.3%	51.1%	
						ϰ =	0.882	OA =	**91.7%**

BRSLKN - LS	2012-2018								
	grassland	built-up	rock	waterbody	broadleaved	mixed	needleleaved	dwarf pine	UA
grassland	**448**	4	4	0	1	0	16	3	94.1%
built-up	1	**60**	0	0	0	1	0	0	96.8%
rock	4	4	**117**	1	0	0	0	0	92.9%
waterbody	0	0	0	**50**	0	0	0	0	100%
broadleaved	0	0	0	0	**31**	12	4	0	66.0%
mixed	0	0	0	0	25	**55**	4	1	64.7%
needleleaved	13	0	2	1	4	30	**702**	24	90.5%
dwarf pine	0	0	0	0	0	1	3	**19**	82.6%
PA	96.1%	88.2%	95.1%	96.2%	50.8%	55.6%	96.3%	40.4%	
						ϰ =	0.858	OA =	**90.1%**

The historical land cover maps from BRs *Salzburger Lungau* and *Kärntner Nockberge* are shown in Figure 19. The strong coniferous forest dominance of the inner alpine forests as well as a more densely populated region in Carinthia and in Salzburg are clearly visible. In particular, when looking at the coniferous forest areas, it is noticeable that from the period 1993-2004 onwards these appear to be significantly sparser than in the previous period 1984-1992.
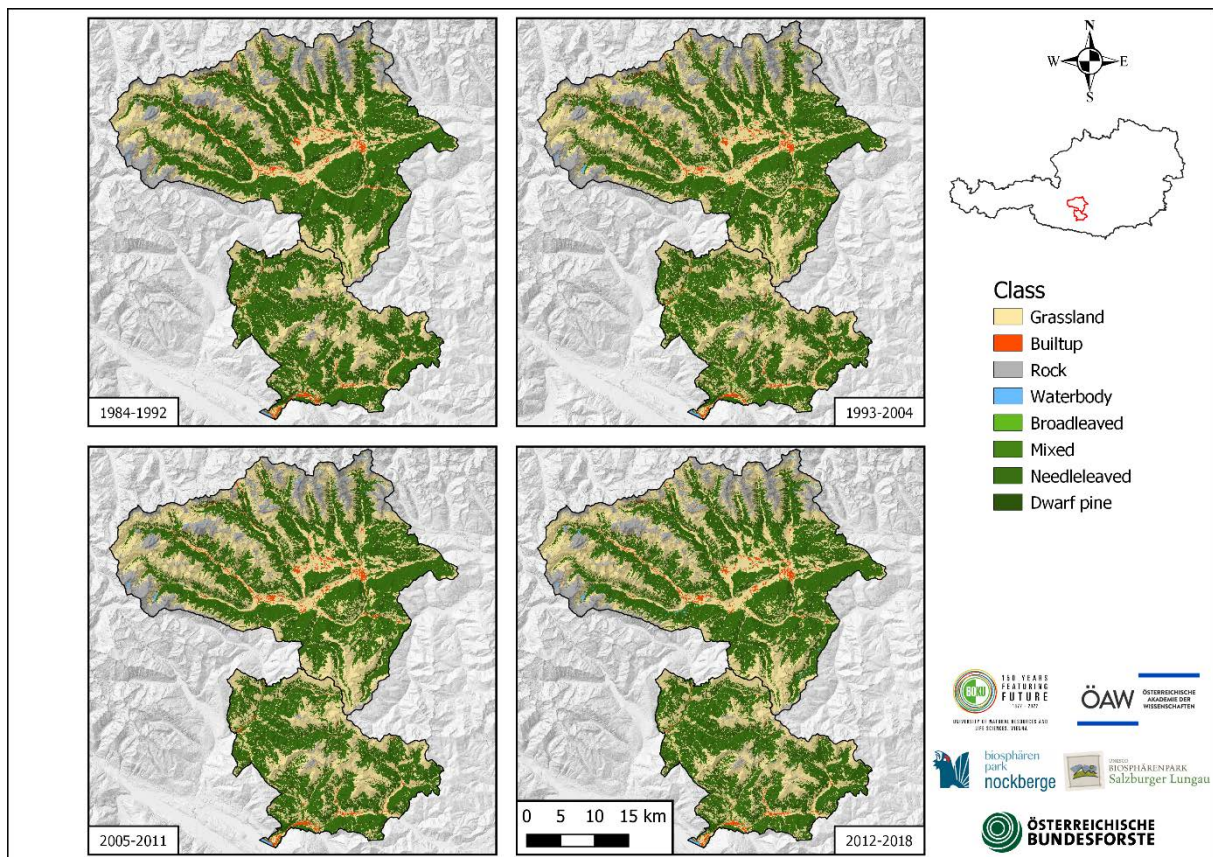

Figure 19: Historical land cover maps of the BRs *Salzburger Lungau* and *Kärntner Nockberge* based on Landsat-imagery.

Diagrams in Figure 20 show the change in land cover classes over time in the three biosphere reserves during the four comparison periods. The originally pixel-based evaluation has already been converted into hectares. It is obvious that the classes are subject to fluctuations over the comparison periods, which can be explained by the inaccuracies of the classification.

The drop of the class coniferous wood in the BRs *Salzburger Lungau* and *Kärntner Nockberge* from the period 1984-1992 to 1993-2004 is striking. If one compares the maps of the periods in this area, it can be concluded that calamity events, caused by the storm event *Uschi* in November 2002, occurred here.
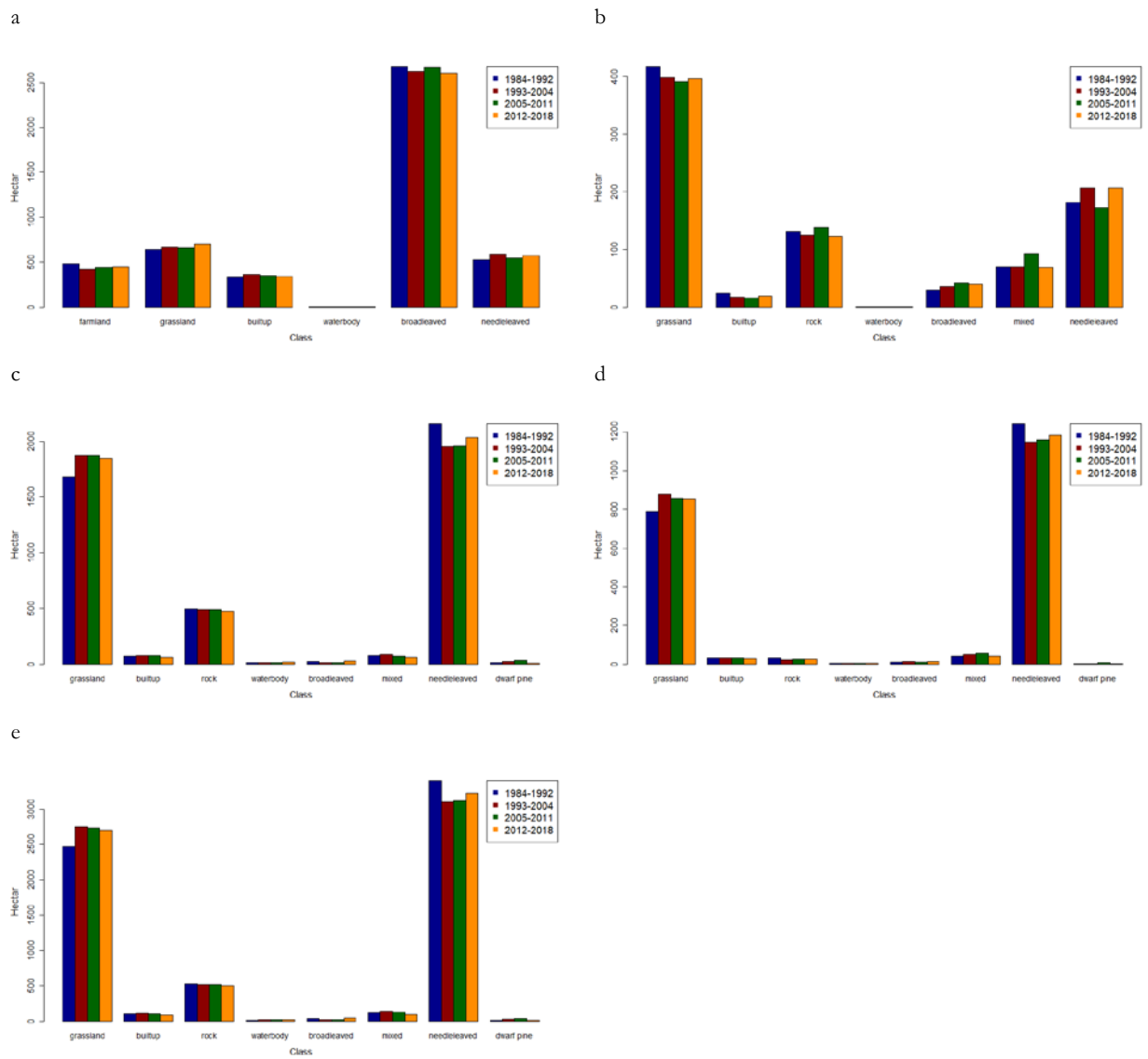
a

b

c

d

e

Figure 20: Change in land cover class over the four comparison periods for all biosphere reserves: (a) BR *Wienerwald*, (b) BR *Großes Walsertal*, (c) BR *Salzburger Lungau*, (d) BR *Kärntner Nockberge* and (e) Joint comparison of the two interconnected BRs *Salzburger Lungau* and *Kärntner Nockberge*.

6. Monitoring possibilities and monitoring concept for all Austrian BRs (WP 6)

In this chapter, various monitoring options of the individual BRs will be explained in more detail. As a biosphere reserve should not only achieve ecological and social goals, but also economic ones, forestry uses play an important role. Figure 21 points out possibilities to identify or quantify these forest uses utilizing satellite data. The difference in the Soil Adjusted Vegetation Index (SAVI) between the year in which the satellite scene was taken and the previous year was calculated, using only one summer scene per year. The greater the difference, the higher the deviation of the green leaf mass of the two points in time. In the time series, as an example and starting from the original condition of the summer of 2017, a clearing colored in yellow can be seen in the following year. This expands towards the north and west in 2019. In the following year, further use is evident along the forest edges in the more northerly area. Since these are coniferous stands and due to the specific characteristics of the use, it can be assumed that this is a forest management activity caused by bark beetle calamity in a secondary coniferous forest.
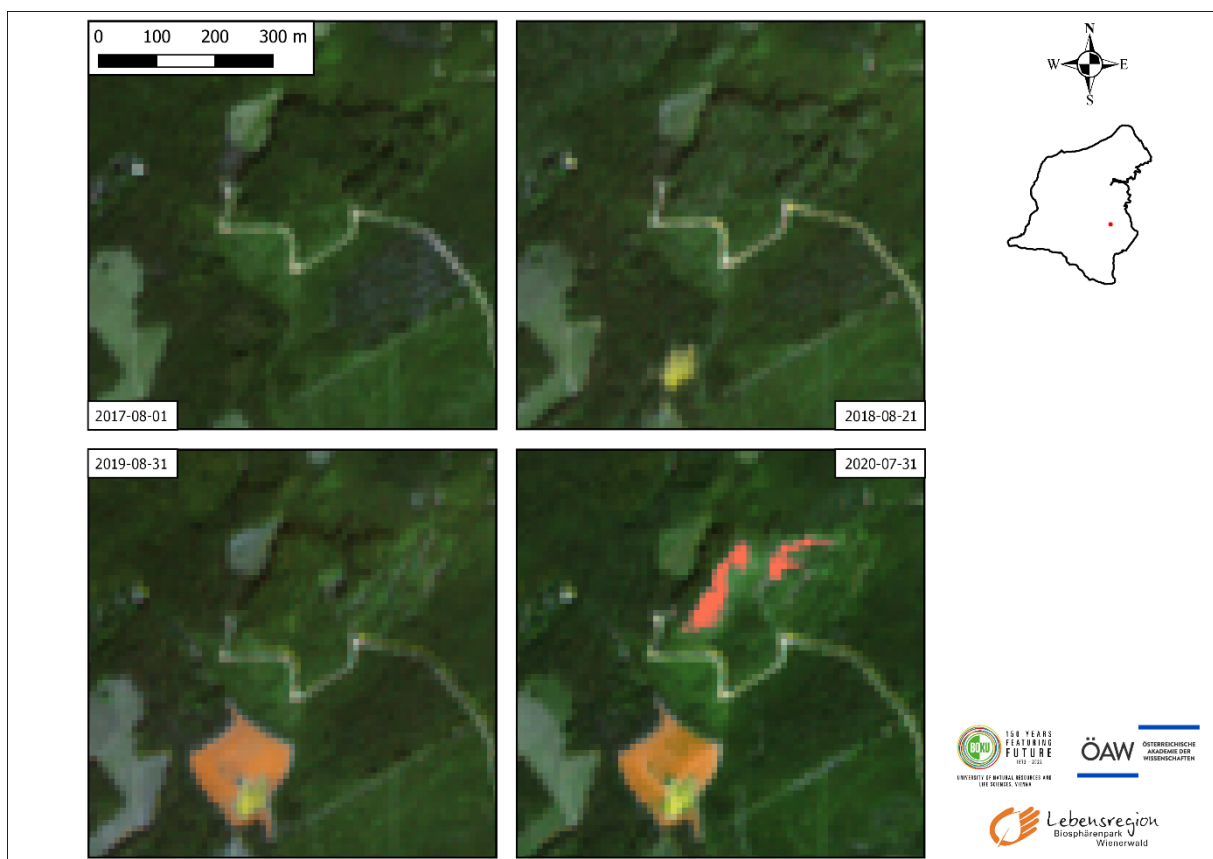

Figure 21: Developing clear-cut, likely caused by bark-beetles. The infestation started in the yellow area and spread to the adjacent coniferous trees to the north (orange). Additional usage is visible on the northern area in the last figure (red).

The following Figure 22 further shows that the SAVI is not only suitable for finding bare areas but is rather a sensitive proxy for green biomass. Thus, it can also be used to monitor and quantify even smaller, non-clear-cut uses such as thinning over a large area.
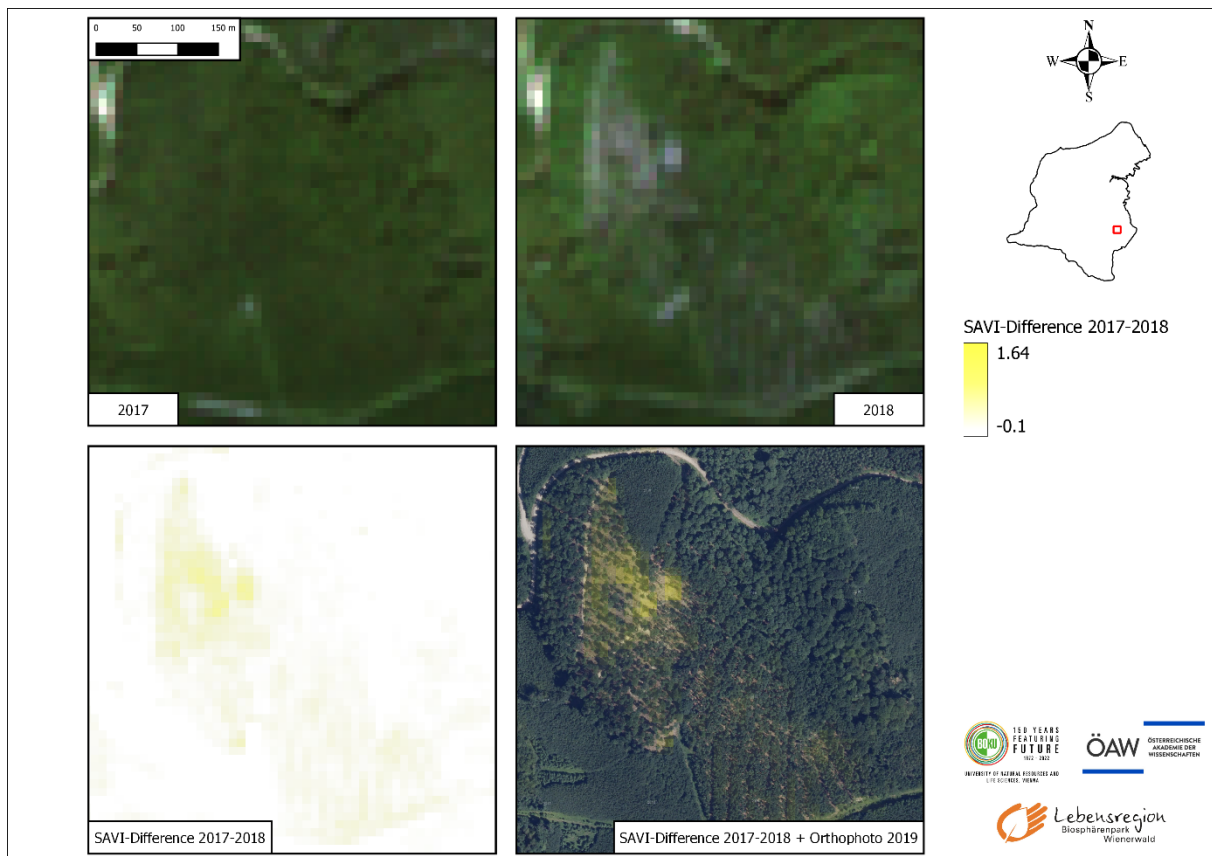
Figure 22: Example of SAVI-responsibility to partial wood crops and thinning of forest canopies due to silvicultural treatments in the BR *Wienerwald*.

Another monitoring possibility is the complete land-use change from one class to another. Figure 23 represents the evolution of a stone pit in the BR *Wienerwald* based on the historical Landsat time series. In the BR *Wienerwald* itself, there is no dedicated class of rock, but due to the spectral similarity, the class built-up can be used as a proxy. In the first period, the young, still relatively small quarry is visible. With further stone mining, a different class is assigned, indicating intensive quarrying. Subsequently, the quarry spreads further and further to the east, with the western, older area becoming increasingly grassy again.

Monitoring can also be done on a larger scale and for specific events in time. As already mentioned in a previous chapter, the storm *Uschi* swept across Western Europe on 16.11.2002 and was responsible for large amounts of damaged wood, especially in the provinces of Carinthia and Salzburg. This impact can be seen clearly in the graphs in the former chapter, but also in Figure 24 a significant land-use change can be recognized. On the left side, the situation before the event shows nearly closed forest areas on the west side of the hillside, whereas the scene on the right-side shows the dramatic loss of wood surface, which passed over from the class needleleaved to the class grassland after the event.
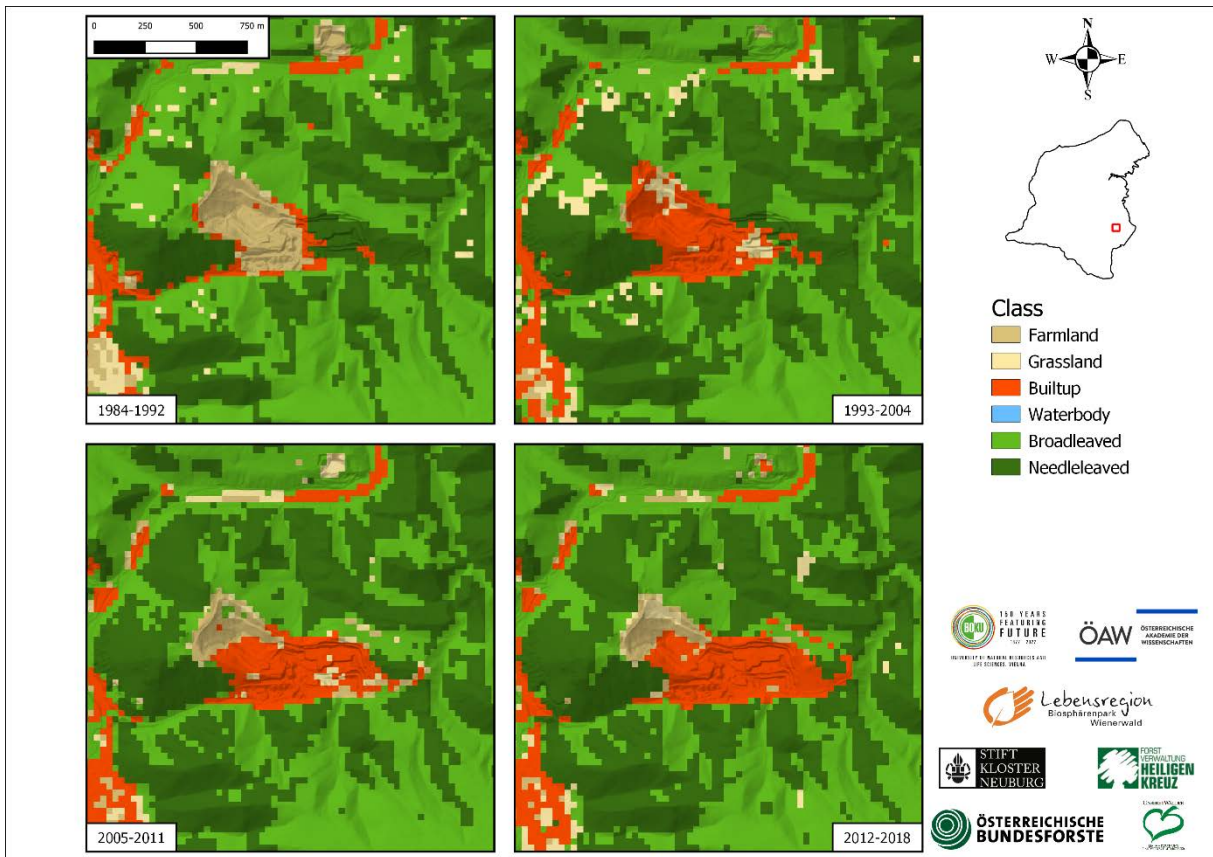
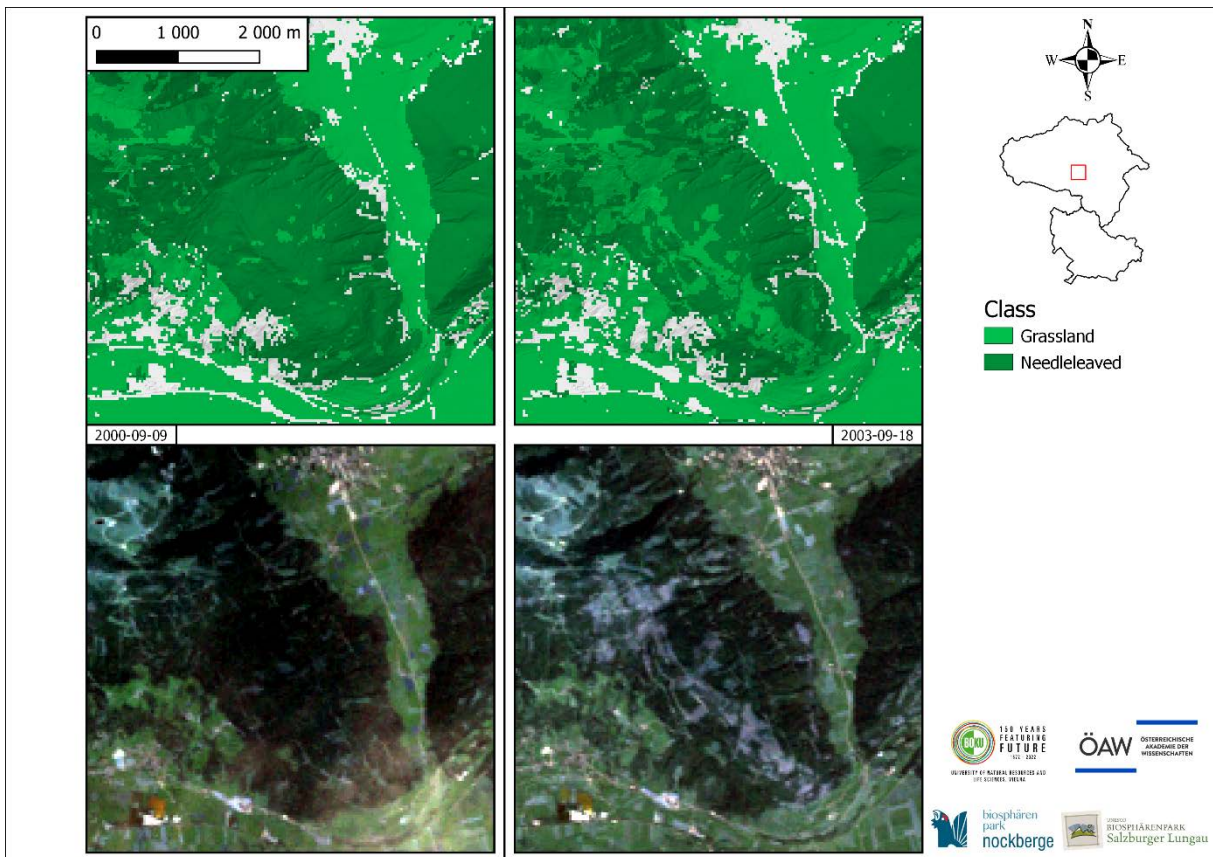Figure 23: Developing of a stone quarry over the four periods in the BR *Wienerwald*.

Figure 24: Impact of the 2002s storm 'Uschi' in the BRs *Salzburger Lungau* and *Kärntner Nockberge*. Wester, wind exposed slopes appear blank after the event.

The accuracies that can be achieved with Sentinel-2 are by far higher than the Landsat-based analysis. This makes it easier to detect and monitor even slow changes such as shrub encroachment. With their high temporal, spatial, and spectral resolution, the two Sentinel-2 satellites provide excellent data for monitoring changes concerning vegetation and will provide a much better representation of the changes analyzed here with Landsat. An ongoing update of the models should be strived for or change analyses directly on the input data can lead to better or more meaningful results. In any case, the classification should be repeated e.g. every three to five years to check whether changes in classes such as tree species can be detected. Shorter intervals have the disadvantage that they are not always guaranteed due to cloud cover. Therefore, more sophisticated methods are needed to detect changes in near real-time, which are currently being researched and will be available soon. In this way, forest management activities but also disturbances in the forest could be recorded quickly. Also, in open areas, it will be useful to carry out continuous analyses to detect changes in the management of mainly sensitive areas. The detailed analyses carried out in the BR *Wienerwald* regarding tree species as well as the analysis of open land management have great potential to be applied to the other BRs. The already described problems concerning data availability (overlapping, frequent clouds, influence of shadows) have to be considered. Nevertheless, useful results can be expected here as well. Especially concerning the analysis of changes, the radar-based Sentinel-1 data have enormous potential, since the temporal sequence is guaranteed. However, for these data, the demanding topography in the mountainous areas is still a big challenge. Finally, it is recommended to all BRs to increase the use of remote sensing data for different purposes, even if not all analyses can be done in-house, the great potential is currently underused. Likewise, many issues not addressed in this project can also be supported by the use of remote sensing. Furthermore, it is recommended to push additional initiatives in the field of reference data, because only with high-quality information from the ground the great potential of earth observation data like Sentinel-2 can be exploited.

7. References

Breiman, L., 2001. Random forests. Mach Learn 45, 5–32. https://doi.org/10.1023/A:1010933404324

EODC GmbH, 2020. Austrian Data Cube [WWW Document]. URL https://acube.eodc.eu/ (accessed 4.1.22).

Féret, J.-B., Asner, G.P., 2014. Mapping tropical forest canopy diversity using high-fidelity imaging spectroscopy. Ecological Applications 24, 1289–1296. https://doi.org/10.1890/13-1824.1

Griffiths, P., Nendel, C., Pickert, J., Hostert, P., 2020. Towards national-scale characterization of grassland use intensity from integrated Sentinel-2 and Landsat time series. Remote Sens Environ, Time Series Analysis with High Spatial Resolution Imagery 238, 111124. https://doi.org/10.1016/j.rse.2019.03.017

Immitzer, M., Böck, S., Einzmann, K., Vuolo, F., Pinnel, N., Wallner, A., Atzberger, C., 2018. Fractional cover mapping of spruce and pine at 1ha resolution combining very high and medium spatial resolution satellite imagery. Remote Sens Environ 204, 690–703. https://doi.org/10.1016/j.rse.2017.09.031

Immitzer, M., Neuwirth, M., Böck, S., Brenner, H., Vuolo, F., Atzberger, C., 2019. Optimal Input Features for Tree Species Classification in Central Europe Based on Multi-Temporal Sentinel-2 Data. Remote Sens 11, 2599. https://doi.org/10.3390/rs11222599